SEMI-ANNUAL PROGRESS REPORT

1 June 1984 1 December 1984

to

National Aeronautics and Space Administration

on

NASA Grant NSG-3264

Entitled

"THE BOUNDARY LAYER ON COMPRESSOR CASCADE BLADES"

Submitted by:

Steven Deutsch and William C. Zierke

Applied Research Laboratory
The Pennsylvania State University
Post Office Box 30
State College, PA 16804

A. INTRODUCTION

The purpose of NASA Research Grant NSG-3264 is to characterize the flow-field about an airfoil in a cascade at chord Reynolds number (R_c) near 5×10^5. The program is experimental and combines laser Doppler anemometry (LDA) with flow visualization techniques in order to obtain detailed flow data [e.g., boundary layer profiles, points of separation and the transition zone] on a cascade of highly-loaded compressor blades. The information provided by this study is to serve as benchmark data for the evaluation of current and future compressor cascade predictive models, in this way aiding in the compressor design process.

This report summarizes the research activity for the period 1 June 1984 through 1 December 1984. Progress made from 1 June 1979 through 1 June 1984 presented in Refs. [1] through [10]. The current report presents the completed pressure surface mean velocity profiles, as well as two detailed near wake velocity profiles, all at a single incidence angle.

B. PROGRESS DURING THE PERIOD 1 JUNE 1984 TO 1 DECEMBER 1984

B.1 Description of the Experiment

The ARL/PSU cascade tunnel is shown in Figure 1. With the current fan system, maximum inlet speed to the cascade section is near 35 m/sec. Inlet turbulence intensity, as measured with a hot-wire anemometer, is below 0.2% as shown in Figure 2. Data to be presented in this report were taken on the pressure surface of a double circular arc compressor blade and in its near wake at a cascade inlet angle of 53° (see Figure 7).

The cascade test section is detailed in Figure 3. It is worth noting that blade pack side suction, as normally employed in cascade testing to maintain two-dimensionality, is not possible because of the need for an LDA

window. Instead, a strong upstream side suction, controllable in the blade-to-blade direction, is employed. Tailboards are used to control the periodicity of the flow.

As current computer codes assume a two-dimensional, periodic cascade flow, data must be taken in such a flow field to be useful. Here, two-dimensionality is taken to imply that the velocities and angles of the flow are substantially the same in spanwise planes, while periodicity means that velocities and flow angles in planes normal to the blades leading and trailing edges are functions only of the distance from a blade (independent of which blade). In a successful two-dimensional, periodic, cascade flow, the ratio of axial velocity from the leading to trailing edge is one. A typical outlet flow profile is shown in Figure 4, the corresponding turning angle in Figure 5, and the blade static pressure distribution in Figure 6. Interpretation of these figures can be facilitated by referring to the definitions of cascade flow angles given in Figure 7. The periodicity of the flow is clearly excellent. Also apparent from the blade pressure distribution is the strong adverse gradient on the suction surface and strong favorable gradient on the pressure surface near the leading edge of the blade. One might then anticipate at this incidence angle, a separation at the leading edge of the suction surface and laminar flow near the leading edge of the pressure surface. The axial velocity ratio, found to be one, is determined by averaging the local axial velocity over three blade passages, centered at the minimum velocity ratio point of the central blade wake. On a day-to-day basis, the variation in axial velocity ratio was within 3%, while the variation in chord Reynolds number was within 1%. A more detailed exposition of the experimental techniques may be found in [11].

A specially designed traversing mechanism which matches the arc of motion of an optics cradle to that of the blade curvature is used for the LDA measurements. All measurements were made in the plane of the local blade normal. Translation of the optics cradle normal to the blade can be accomplished in step intervals as small as 0.0254 mm. Prior to LDA measurements, a reference distance was established by focusing the LDA control volume on an insert which fit over the central measuring blade. Narrow lines are etched on the insert so as to be at known locations from the blade surface. Repeatability in establishing a measurement reference was estimated to be ± 0.05 mm, and this uncertainty is probably the major source of scatter in the velocity data.

A schematic of the LDA optics system is shown in Figure 8. A two Watt Spectra-Physics Argon-Ion laser was used for the measurements. Power on the blue line employed (488 nm) ranged between 0.6 to 0.8 Watts. Standard TSI backscatter optical components were used: the focusing lens (focal distance = 371.3 mm) allowed the measurements to be made at the blade mid-span. The focal volume was ellipsoidal and was predicted to be 0.56 mm × 0.037 mm in the direction normal to the blade. Optical shifting at 5 Mhz was employed. To measure close to the surface the optical cradle was tilted 1°. Silicon carbide particles having a mean diameter of 1.5 μm were used for laser seeding. In an attempt to maintain a uniform distribution, seed was injected well upstream of the measurement station (see Figure 1) at the flexible coupling.

LDA data acquisition and reduction was accomplished by using a direct link to a VAX 11/782 computer. Software allowed selection of focusing lens half angle, laser wavelength, frequency shift, minimum cycles employed in the calculation and number of particle counts per run (up to 4000). Initial

output was in the form of a velocity histogram. Minimum and maximum velocity limits were set by a cursor from the histogram to eliminate obvious noise. Final output was mean velocity, turbulence intensity and percent of particle counts employed in the calculation. The latter served as a signal-to-noise indicator. It is probably fair to state that at least 98% of the total particle counts were employed for measurement stations in the boundary layer; at least 95% were employed for points in the free stream. Mean velocity here was taken as a simple arithmetric average

$$u = \frac{1}{N} \sum_{n=1}^{N} u_n \quad , \tag{1}$$

and local turbulence intensity (L.T.I.) as

$$\frac{u'}{u} = \frac{1}{u} \frac{1}{N} \sum_{n=1}^{N} (u_n - u)^2 \; ^{1/2} \tag{2}$$

Experience has shown that quite satisfactory repeatability of the mean and turbulence intensity can be guaranteed in boundary layer flows by using N = 1000 particle counts in regions in which the L.T.I. exceeds 5%, 500 points for L.T.I. less than 5% and 200 points for the free stream. At each measurement station, profiles were defined by statistically treating the data for six individual experiments. Error bands, presented on each plot, represent 95% confidence levels as determined by a student T-test.

The preliminary data analysis is automated on the ARL/VAX computer. The effects of normal pressure gradient are accounted for first. Details of the technique are given in Reference [11] and are equivalent to that used by Ball, et.al. [12] and Mellor, et.al. [13]. Briefly the technique assumes that the profile may be represented as

$$u_{meas} = u_{BL} + u_{inv} - U_e \tag{3}$$

so that the edge velocity (U_e) can be determined by extrapolating the outer inviscid flow (u_{inv}) to the wall (where $u_{meas} = u_{BL} = 0$) in some reasonable manner. The reconstructed boundary layer can then be analyzed in several ways. For example, the mean profiles can be fit to Cole's composite profile [14] or compared to a Falkner-Skan profile [15] (at equivalent pressure gradient). For all the measured profiles, integral parameters can also be calculated from a smooth cubic spline fit. Finally, skin friction calculations can also be made, where appropriate, using the Ludwig-Tilman [15] correlations.

B.2 Results and Discussion

Eleven profiles were measured on both the pressure and suction surfaces of the double circular arc blades; two profiles were measured in the near wake. Each profile contains mean velocity and turbulence intensity information; for most of the profiles, the skewness and kurtosis was also calculated. Profiles taken at the first seven chord locations on the suction surface were presented and analyzed in References [10] and [11]. The last four (separated) profiles were presented without analysis in Reference [10] and again with brief discussion in Reference [12]. The current progress report describes the pressure surface and near wake data. Analysis of all the data is continuing and a journal article is planned.

The pressure surface pressure gradient was plotted in Figure 6. It is somewhat more physically satisfying to present these pressure data in terms of an edge velocity and this is done in Figure 9. Note the strong acceleration at the leading edge. The pressure gradient and edge velocity change continuously with chord location so that equilibrium boundary layers cannot be expected here. The strong favorable gradient (or the acceleration) at the leading edge suggests a region of laminar flow. In these laminar flow

regimes, we might anticipate that Falkner-Skan profiles may apply locally -- provided of course, that the blade static pressure is changing slowly enough.

The displacement thickness δ^* and the shape factor H for the pressure surface boundary layer profiles are shown in Figure 10. All the results shown in Figure 10 are based on a smooth cubic spline fit of the boundary layer profiles with the exception of the shape factor calculations at 2.7, 5.9 and 14.4% chord. Because of the lack of near wall measurements for these extremely thin layers, a spline fit was not felt to be accurate and the H values were calculated from the appropriate Falkner-Skan profile (based on the local pressure gradient and the approach velocity). It is perhaps worth noting here that the smallest displacement thickness (at 2.7% chord) is only twice the ideal LDA length scale in the gradient direction, and that the maximum displacement thickness of 0.83 mm at 57.2% chord is about the same as that encountered near the leading edge of the suction surface. The shape factor H indicates a boundary layer passing from laminar to turbulent; although the combination of pressure gradient and elevated free-stream turbulence intensity make direct use of this information to, say, predict the transition point impractical.

The eleven velocity profiles are presented in dimensional form in Figures (11) through (21). Here the pentagons represent the averaged data and the triangles the boundary layer profiles, reconstructed with the effect of the normal pressure gradient removed. For all but the plot at 97.6% chord, the dashed line represents the extrapolation of the inviscid region to the wall to determine U_e. No measureable normal pressure gradient was observed at 97.9% chord so that the pentagons and triangles are identical. Note the significant curvature in the mean profile at both 2.7 and 5.9% chord. Similar inviscid

curvature was noted near the leading edge on the suction surface; the effect is no doubt due to the strong response of the flow (streamline bending) upon encountering the blocking effect of the blades. As in all results shown, the error bands represent 95% confidence levels as determined by the student T-test. At 2.7 and 5.9% chord, the LDA could only make a nominal penetration of the boundary layer so that the resolution of the profiles at these locations is not good.

The boundary layer mean velocity profiles are replotted non-dimensionally in Figures 22 to 32. Also shown on these figures are the Falkner-Skan velocity profiles based on the approach velocity, local chord length and local pressure gradient. The Falkner-Skan plots appear to be a reasonable estimate of the mean profile data through about 57.2% chord. At 68% chord and beyond, there is an increasing thickening of the profile relative to the Falkner-Skan correlation, which may indicate a transitioning boundary layer. It should be noted that preliminary flow visualization studies indicate that transition occurs near 70% chord -- that is, in reasonable agreement with our interpretation of the data. In the sense that a logarithmic region might be interpreted as indicating a transitioning or turbulent boundary layer, it is important to note that a logarithmic layer is not observed for any of the profiles on the pressure surface. This is not surprising, however, as R_θ never gets above 700 here; moreover, the convex curvature no doubt acts to suppress the turbulence (see, for example [16]).

Although the prediction of the initiation of transition as beginning near 70% chord is attractive from interpretation of the mean profile data, the turbulence intensity profiles do not support this conclusion. Consider a plot (Figure 23) of the turbulence intensity versus chord location for a constant Y location of 0.0381 cm above the blade. Again the peak of the turbulence

intensity profile is in reasonable agreement with our earlier prediction of transition near 70% chord; however, intensities as high as 7% even at 2.7% chord are not consistent with the existence of laminar flow near the leading edge. This point may be reinforced by examining the turbulence intensity profile at 25% chord (say as is done in Figure 24). Although the mean profile (see Figures 14) is laminar like, the intensity is much too high in the layer for this to be consistent with a laminar boundary layer.

Understanding of this phenomenon is not complete. It seems likely that the "extra" turbulence intensity arises because of a general flow unsteadiness caused by the massive time dependent suction surface separation. This supposition, however, cannot be verified using "low sample rate" LDA measurements alone, but requires the examination of data continuous in time. To this end, both flush-mounted, hot-film probes (as an uncalibrated transition indicator) and a traversable hot-wire probe will be inserted into the pressure surface flow field.

Detailed wake profiles at 105.4 and 109.6% chord are shown in Figures 25 and 26. All data are taken relative to an extension of the pressure surface circular arc. That is, all profiles are normal to this arc, the position $y = 0$ represents the extension of the pressure surface along its arc, and $y > 0$ represents distances off the pressure surface. Data analysis of the wake region is just beginning. Clearly the regions of significant backflow will be of some interest here.

C. GOALS FOR THE NEXT REPORTING PERIOD

During the next six-month period, it is anticipated that:

- Flow visualization studies will be completed.
- Data analysis will be completed and a journal article based on the results submitted.

C. GOALS FOR THE NEXT REPORTING PERIOD Cont'd)

- A presentation of the results will be made at NASA-Lewis.
- Flow studies at a second incidence will be underway.

D. REFERENCES

[1] Deutsch, S., Semi-Annual Progress Report for NASA Grant NSG-3264, January 1980.

[2] Deutsch, S., Semi-Annual Progress Report for NASA Grant NSG-3264, June 1980.

[3] Deutsch, S., Semi-Annual Progress Report for NASA Grant NSG-3264, January 1981.

[4] Deutsch, S., Semi-Annual Progress Report for NASA Grant NSG-3264, June 1981.

[5] Deutsch, S., Semi-Annual Progress Report for NASA Grant NSG-3264, January 1982.

[6] Deutsch, S., Semi-Annual Progress Report for NASA Grant NSG-3264, June 1982.

[7] Deutsch, S. and S. Gearhart, Semi-Annual Progress Report for NASA Grant NSG-3264, December 1982.

[8] Deutsch, S., Semi-Annual Progress Report for NASA Grant NSG-3264, May 1983.

[9] Deutsch, S. and W. C. Zierke, Semi-Annual Progress Report for NASA Grant NSG-3264, December 1983.

[10] Deutsch, S. and W. C. Zierke, Semi-Annual Progress Report for NASA Grant NSG-3264, June 1984.

D. REFERENCES (Cont'd)

[11] Deutsch, S. and W. C. Zierke, "Some Measurements of Boundary Layers on the Suction Surface of Double Circular Arc Blades in Cascades," ARL/PSU TM 84-77, Applied Research Laboratory, The Pennsylvania State University (3 April 1984).

[12] Ball, C. L., L. Reid and J. F. Schmidt, "End-Wall Boundary Layer Measurements in a Two Stage Fan," NASA TM 83409 (June 1983).

[13] Mellor, G. L. and G. M. Wood, "An Axial Compressor End-Wall Boundary Layer Theory," Trans. of Basic Engr., Journal of Basic Engr. (June 1971).

[14] Coles, D. E. and E. A. Hirst, "Computation of Turbulent Boundary Layers," Proceedings of the 1968 AFOJR-IFP-Stanford Conference.

[15] White, F. M., Viscous Fluid Flow, McGraw-Hill, Inc. (1974).

[16] So, R. M. L., "A Turbulence Velocity Scale for Curved Shear Flows," J.F.M., Vol. 70, pp. 37-57 (1975).

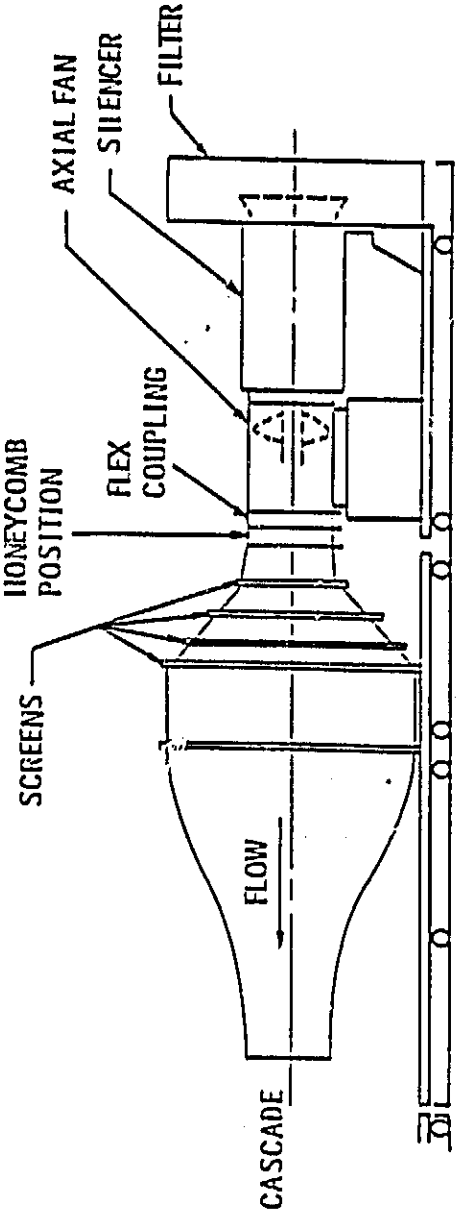
FILTER
SILENCER
AXIAL FAN
FLEX COUPLING
HONEYCOMB POSITION
SCREENS
FLOW
CASCADE

Figure 1.

Figure 2.

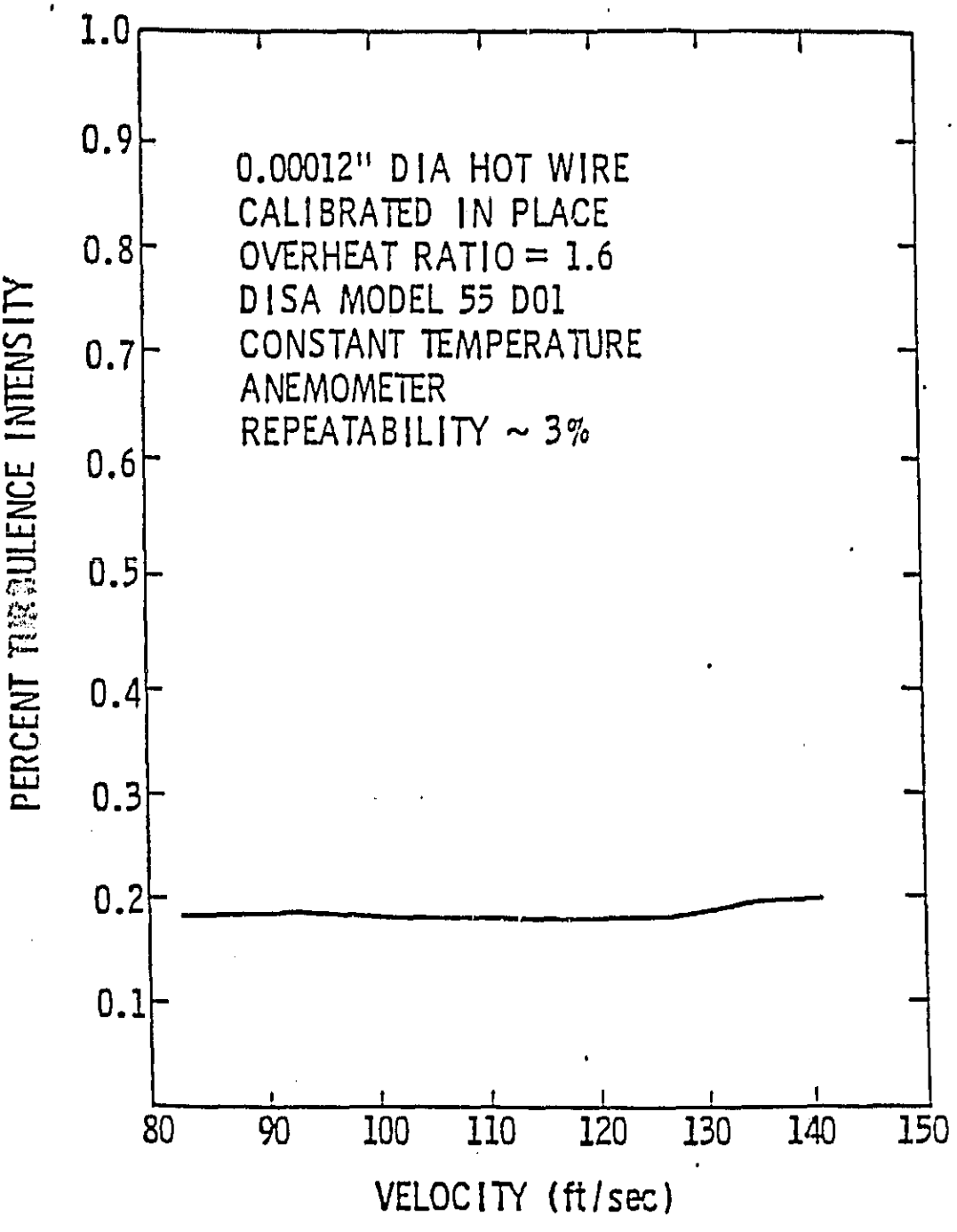
1.0
0.9
0.8
0.7
0.6
0.5
0.4
0.3
0.2
0.1
0.00012" DIA HOT WIRE
CALIBRATED IN PLACE
OVERHEAT RATIO = 1.6
DISA MODEL 55 D01
CONSTANT TEMPERATURE
ANEMOMETER
REPEATABILITY ~ 3%
PERCENT TURBULENCE INTENSITY
80
90
100
110
120
130
140
150
VELOCITY (ft/sec)

Figure 3.

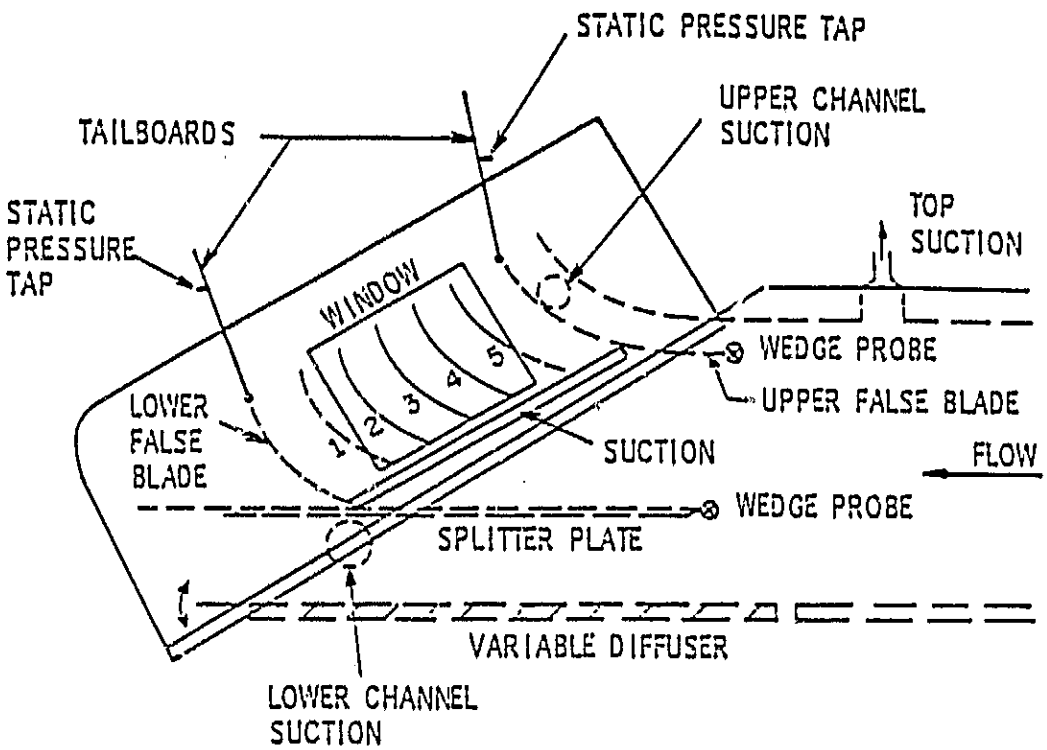
STATIC PRESSURE TAP
UPPER CHANNEL SUCTION
TAILBOARDS
STATIC PRESSURE TAP
TOP SUCTION
WINDOW
1
2
3
4
5
WEDGE PROBE
UPPER FALSE BLADE
LOWER FALSE BLADE
SUCTION
FLOW
WEDGE PROBE
SPLITTER PLATE
VARIABLE DIFFUSER
LOWER CHANNEL SUCTION

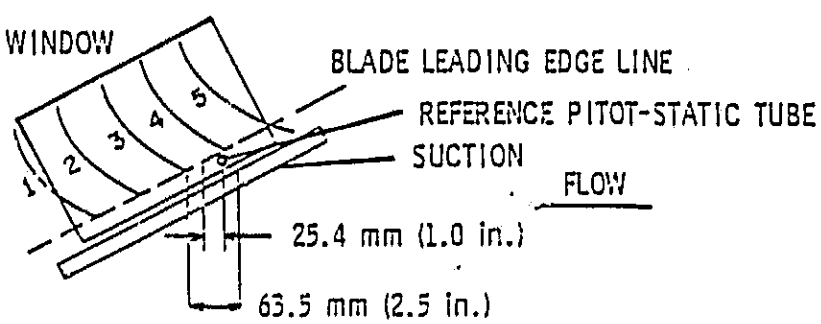
WINDOW
BLADE LEADING EDGE LINE
REFERENCE PITOT-STATIC TUBE
SUCTION
FLOW
1
2
3
4
5
25.4 mm (1.0 in.)
63.5 mm (2.5 in.)

Figure 4.

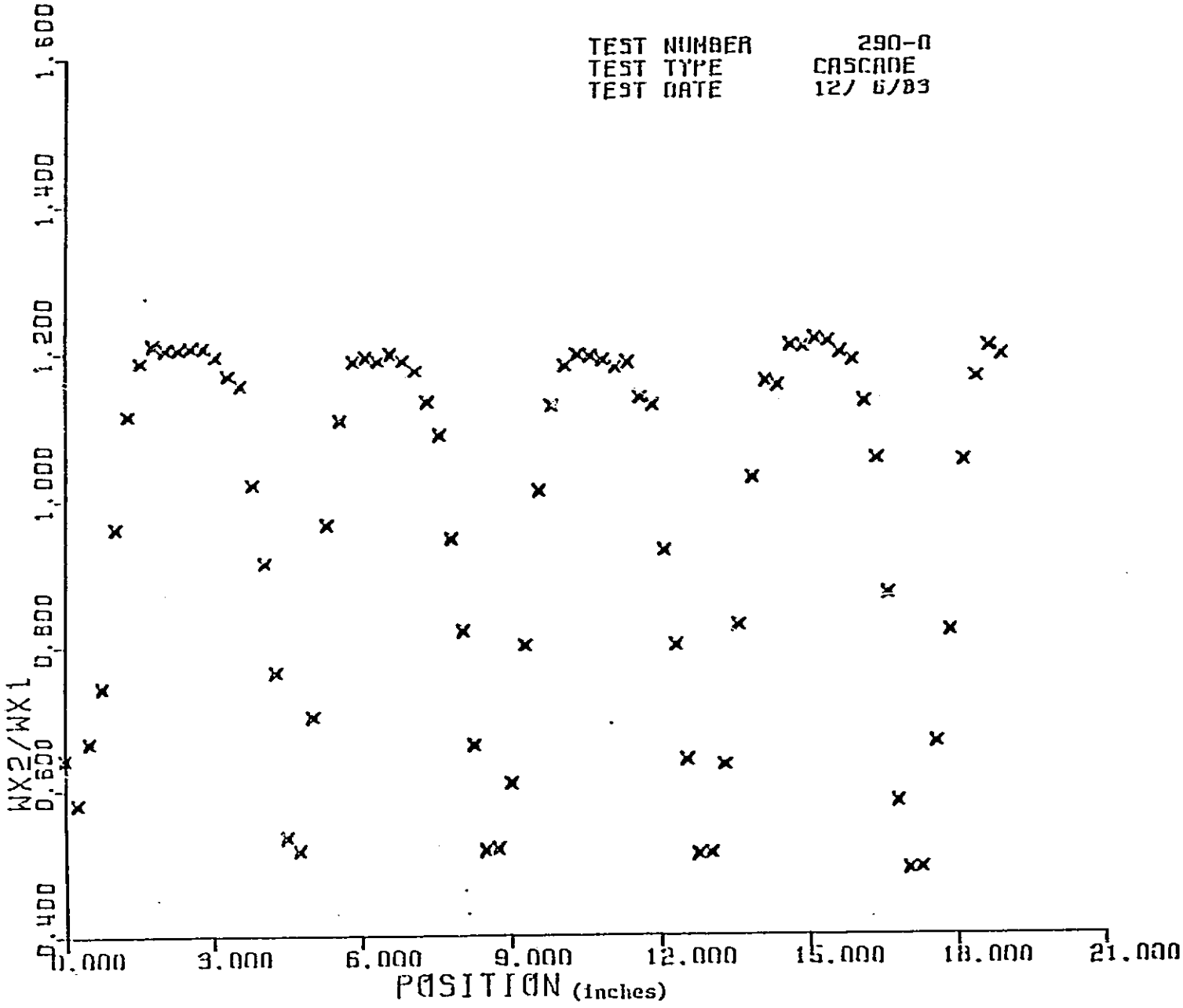
TEST NUMBER 290-0
TEST TYPE CASCADE
TEST DATE 12/ 6/83
WX2/WX1
1.600
1.400
1.200
1.000
0.800
0.600
0.400
0.000
3.000
6.000
9.000
12.000
15.000
18.000
21.000
POSITION (inches)

Figure 5.

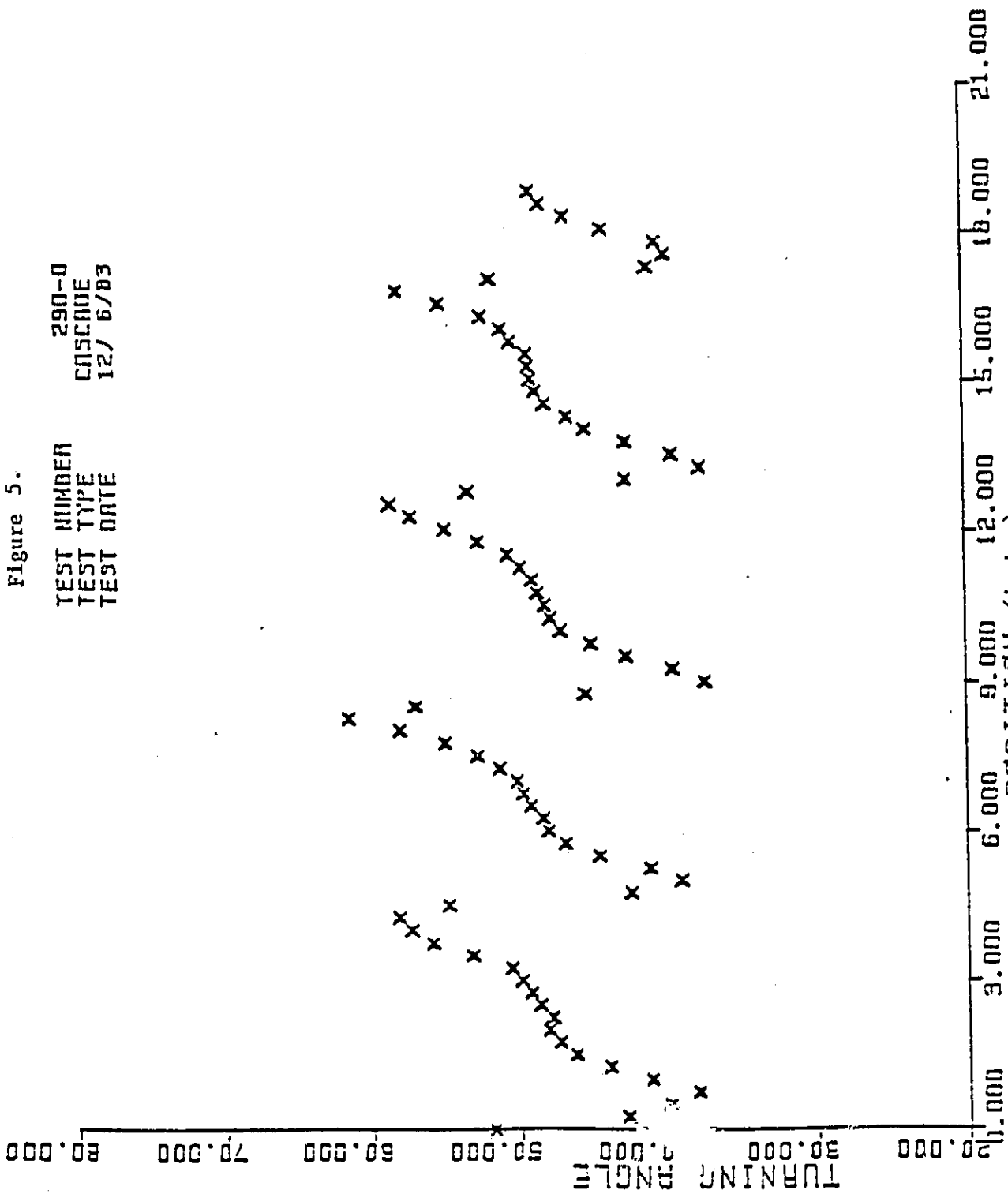
TEST NUMBER 290-0
TEST TYPE CASCADE
TEST DATE 12/ 6/83
TURNING ANGLE
0.000
30.000
60.000
90.000
0.000
3.000
6.000
9.000
12.000
15.000
18.000
21.000
POSITION (inches)

Figure 6.

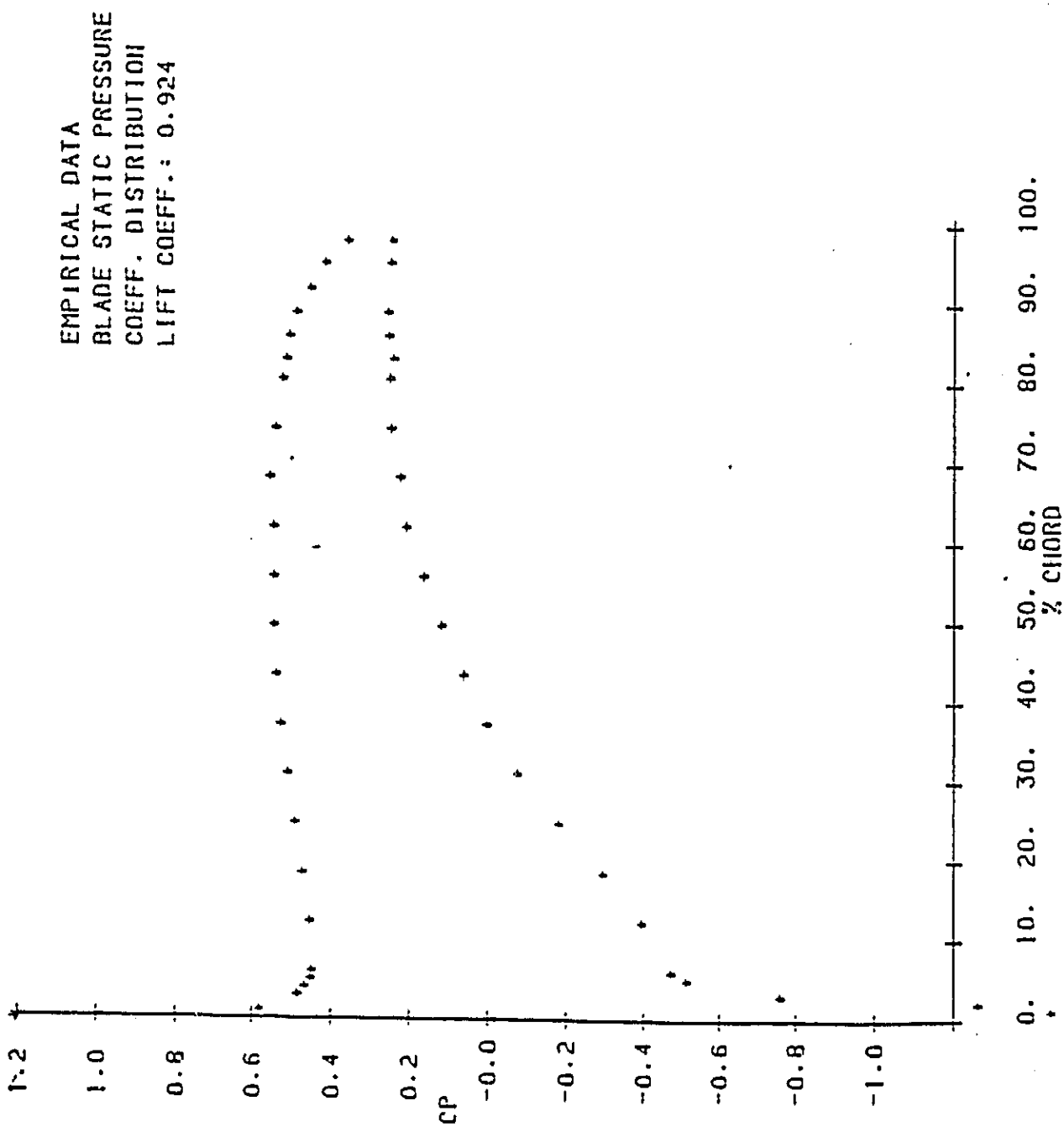
EMPIRICAL DATA
BLADE STATIC PRESSURE
COEFF. DISTRIBUTION
LIFT COEFF.: 0.924
1.2
1.0
0.8
0.6
0.4
0.2
-0.0
-0.2
-0.4
-0.6
-0.8
-1.0
CP
0.
10.
20.
30.
40.
50.
60.
70.
80.
90.
100.
% CHORD

Figure 7.

CASCADE ANGLES

W1	INLET VELOCITY
W2	OUTLET VELOCITY
β_1	INLET FLOW ANGLE
β_2	OUTLET FLOW ANGLE
WX1	INLET AXIAL VELOCITY
WX2	OUTLET AXIAL VELOCITY

TURNING ANGLE $\theta = \beta_1 + \beta_2$

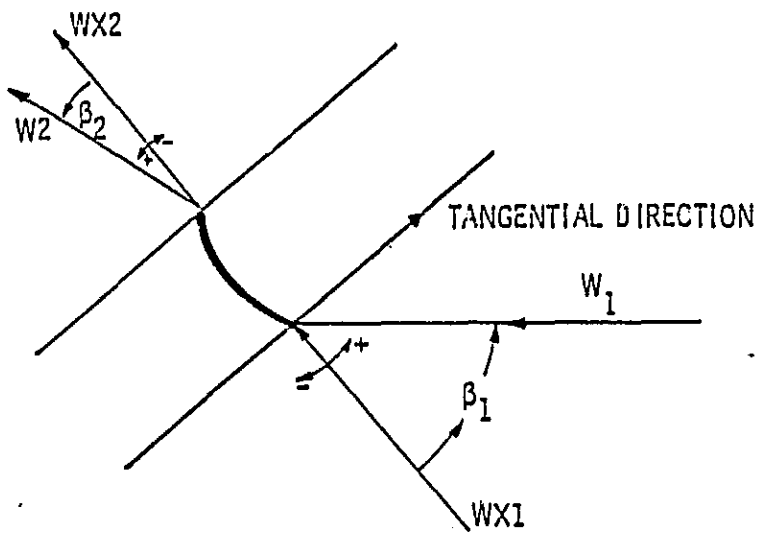

Figure 8.

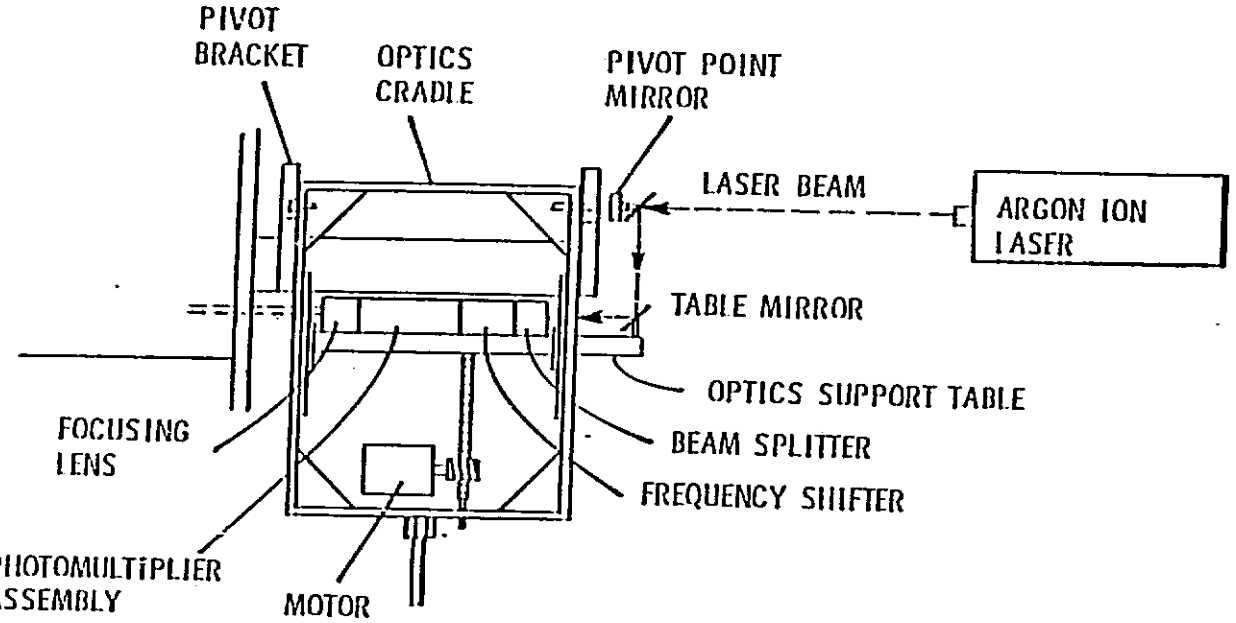
PIVOT
BRACKET
OPTICS
CRADLE
PIVOT POINT
MIRROR
LASER BEAM
ARGON ION
LASER
TABLE MIRROR
OPTICS SUPPORT TABLE
FOCUSING
LENS
BEAM SPLITTER
FREQUENCY SHIFTER
PHOTOMULTIPLIER
ASSEMBLY
MOTOR

Figure 9.

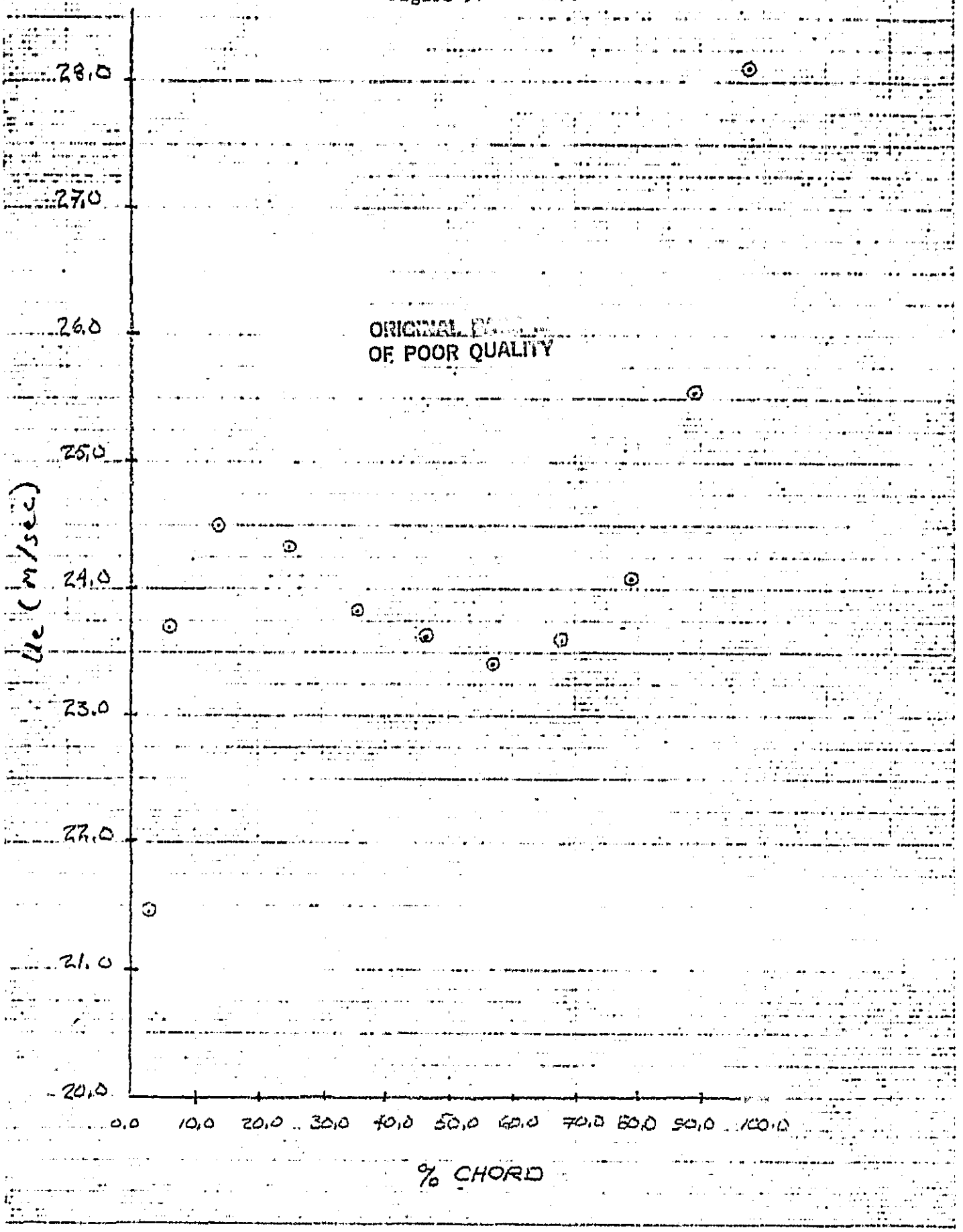

Figure 10.

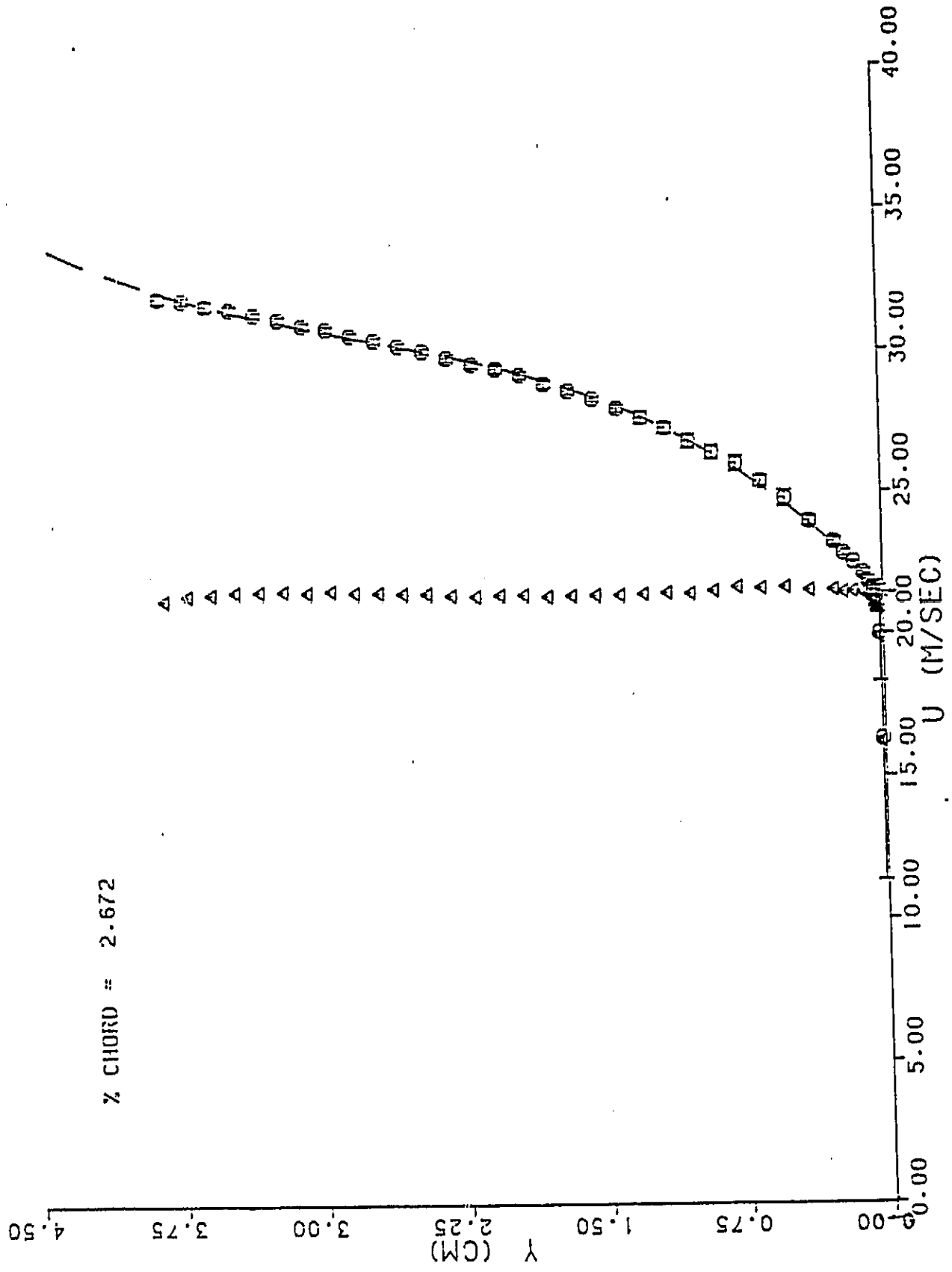
% CHORD = 2.672
0.00
5.00
10.00
15.00
20.00
25.00
30.00
35.00
40.00
U (M/SEC)
0.00
0.75
1.50
2.25
3.00
3.75
4.50
Y (CM)

Figure 11.

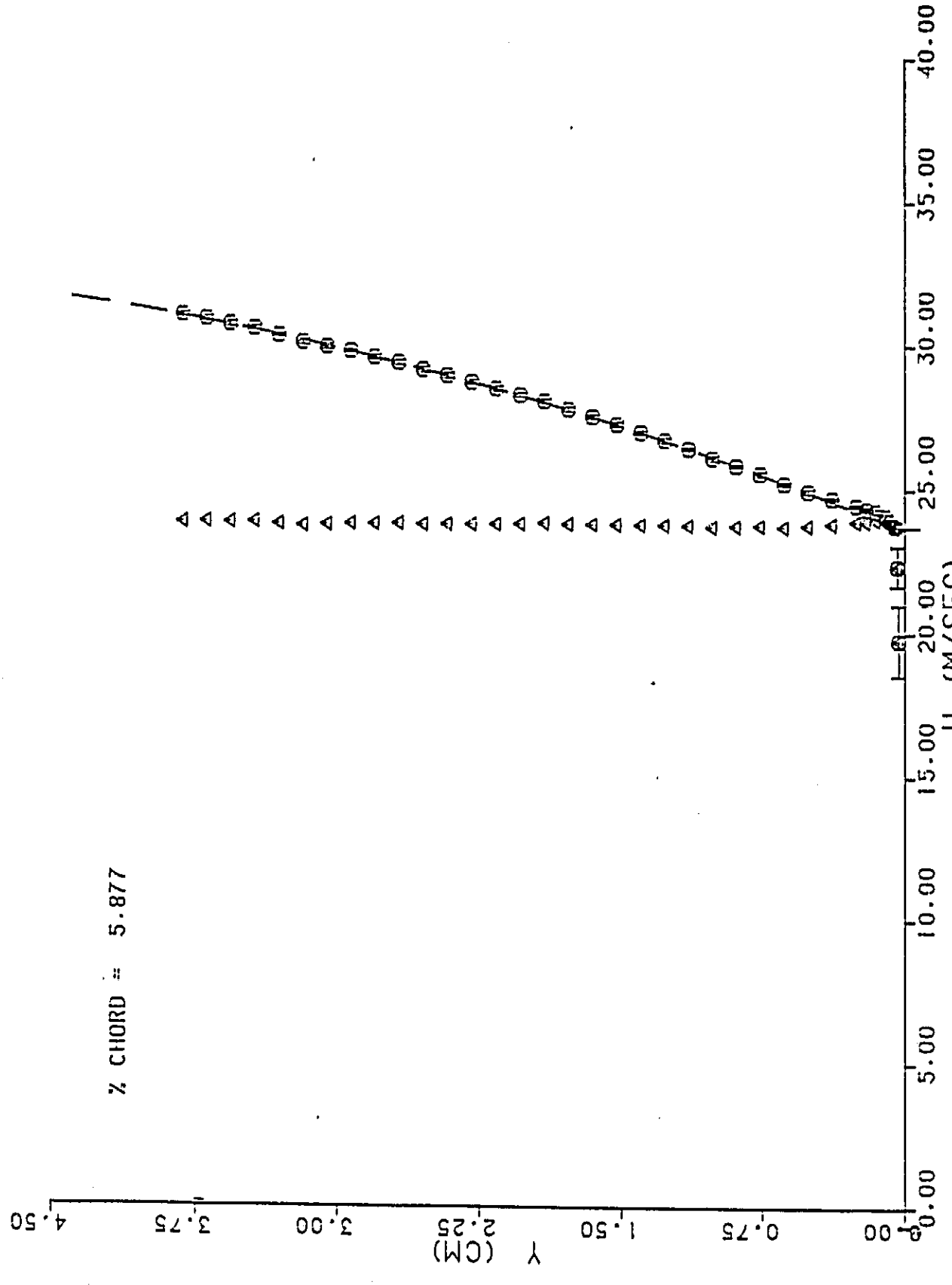
% CHORD = 5.877
Y (CM)
0.00
0.75
1.50
2.25
3.00
3.75
4.50
U (M/SEC)
0.00
5.00
10.00
15.00
20.00
25.00
30.00
35.00
40.00

Figure 12.

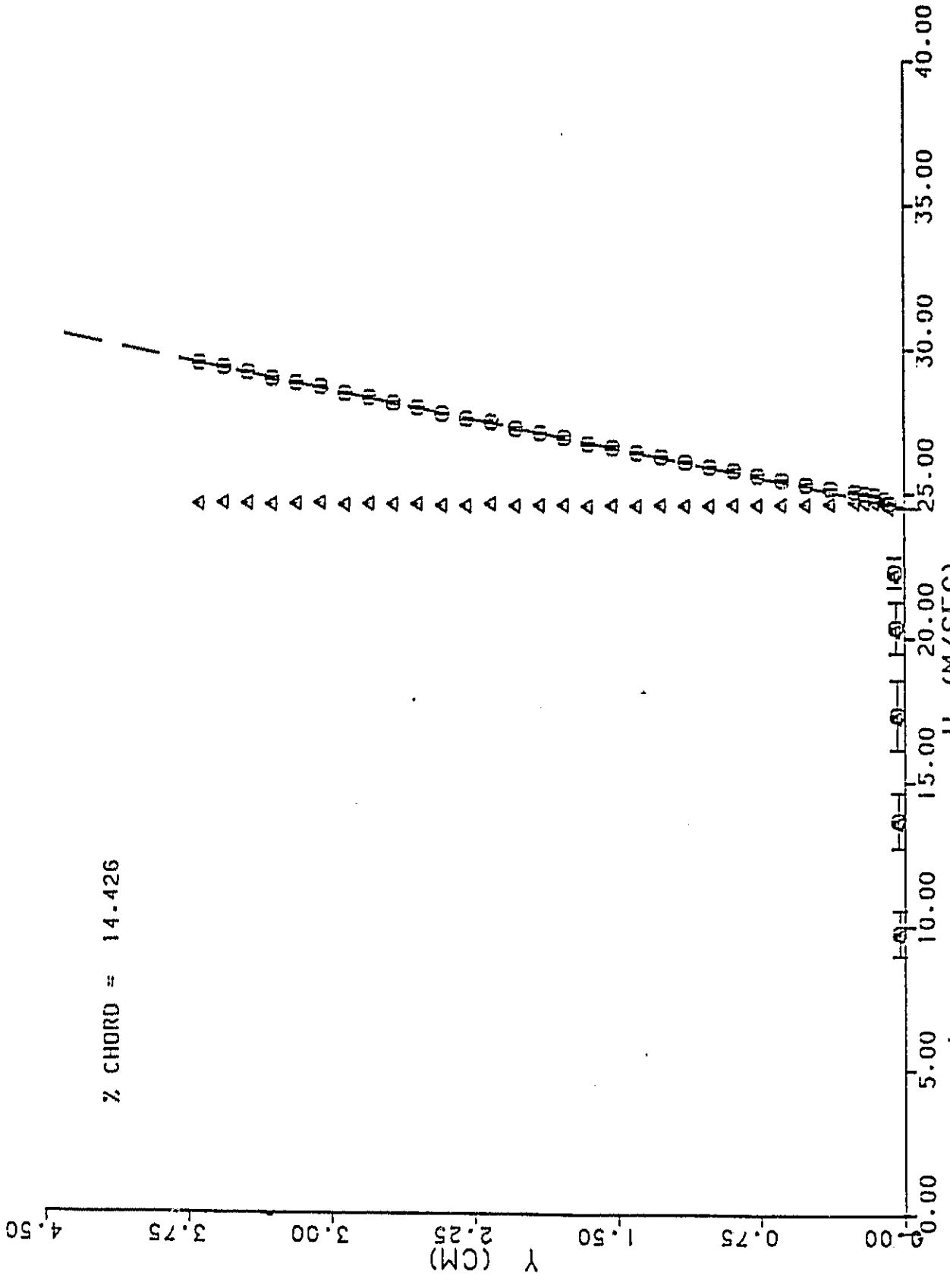
% CHORD = 14.426
Y (CM)
0.00
0.75
1.50
2.25
3.00
3.75
4.50
U (M/SEC)
0.00
5.00
10.00
15.00
20.00
25.00
30.00
35.00
40.00

Figure 13.

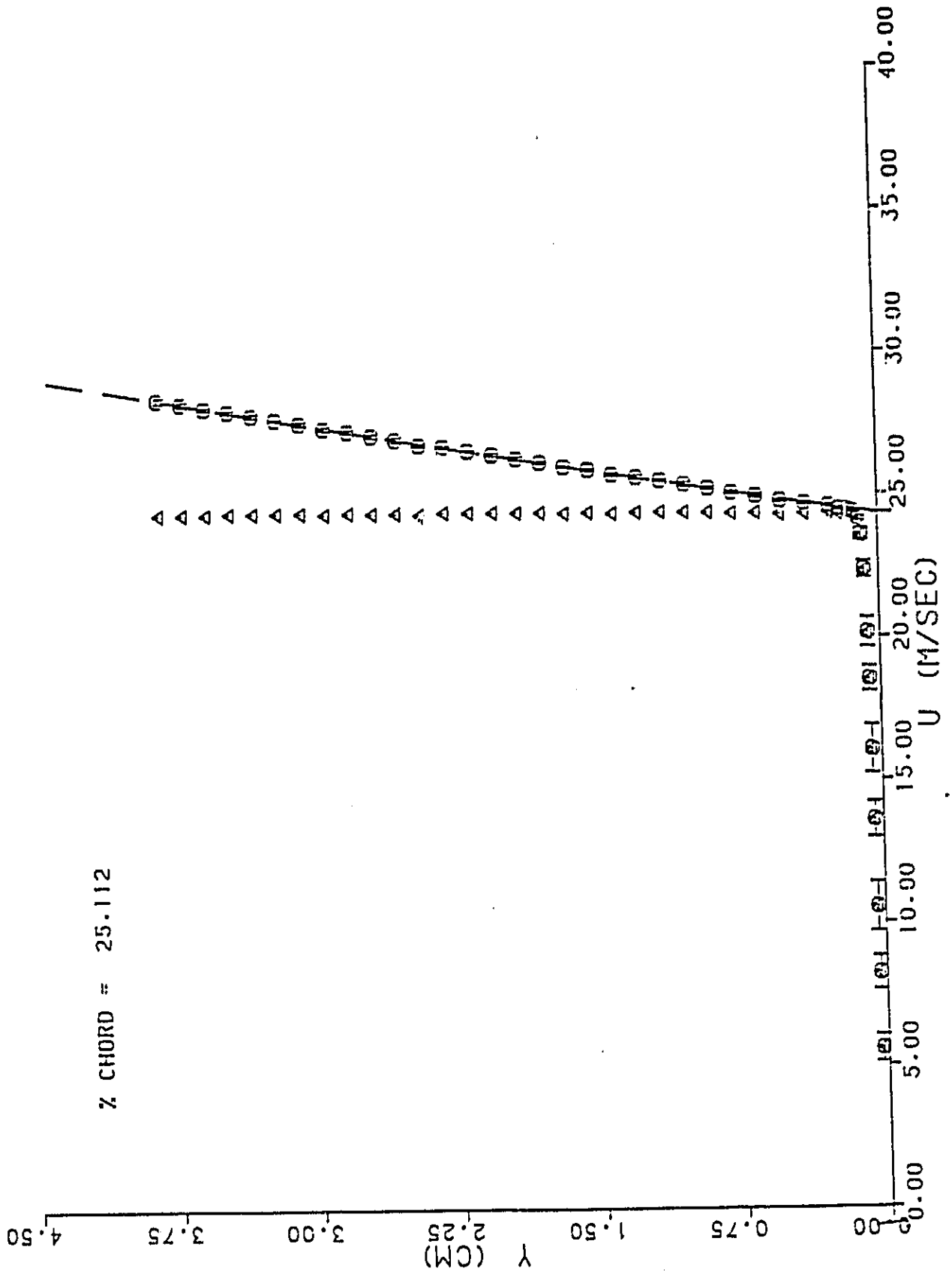
% CHORD = 25.112
Y (CM)
U (M/SEC)
0.00
0.75
1.50
2.25
3.00
3.75
4.50
0.00
5.00
10.00
15.00
20.00
25.00
30.00
35.00
40.00

Figure 14.

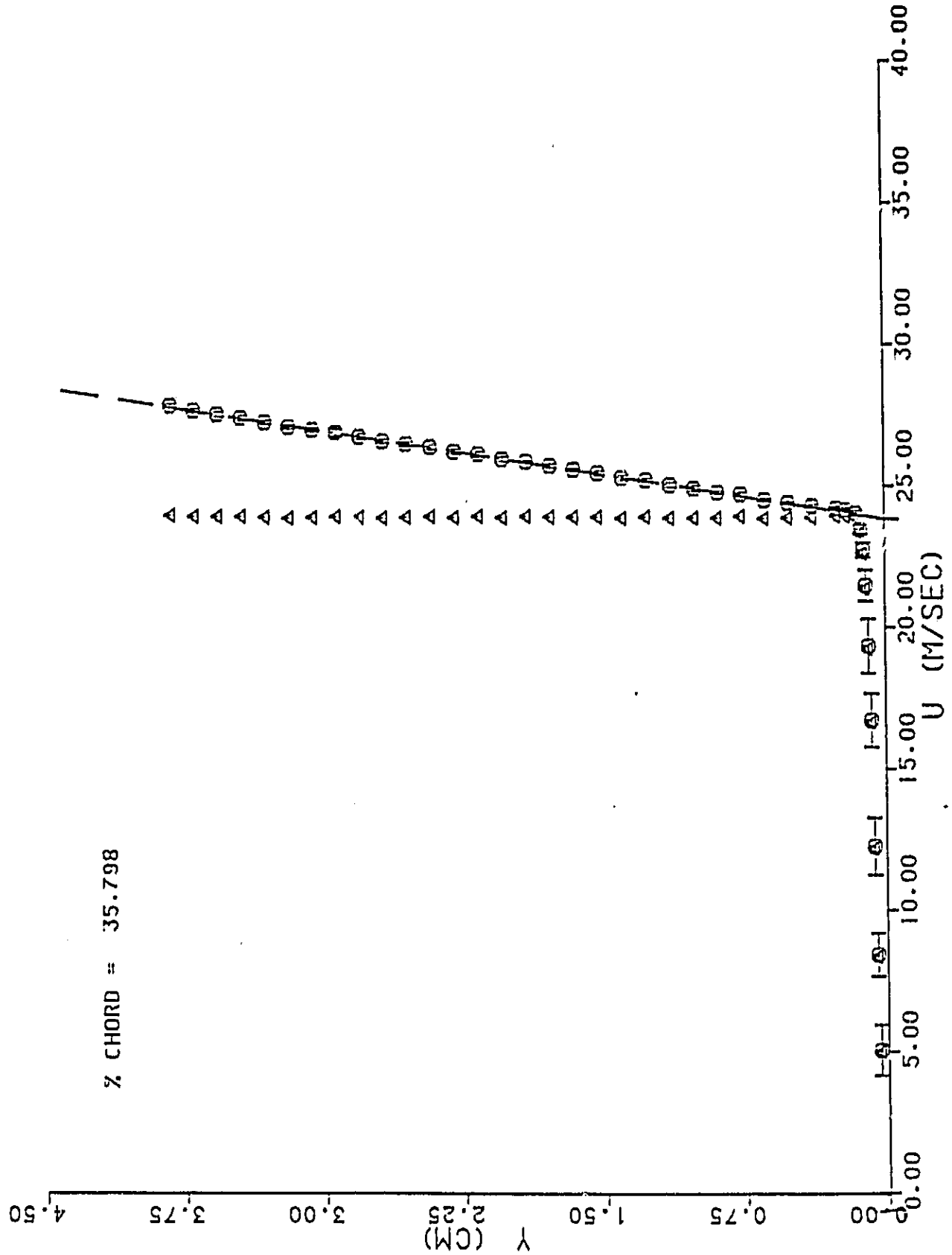
% CHORD = 35.798
Y (CM)
0.00
0.75
1.50
2.25
3.00
3.75
4.50
U (M/SEC)
0.00
5.00
10.00
15.00
20.00
25.00
30.00
35.00
40.00

Figure 15.

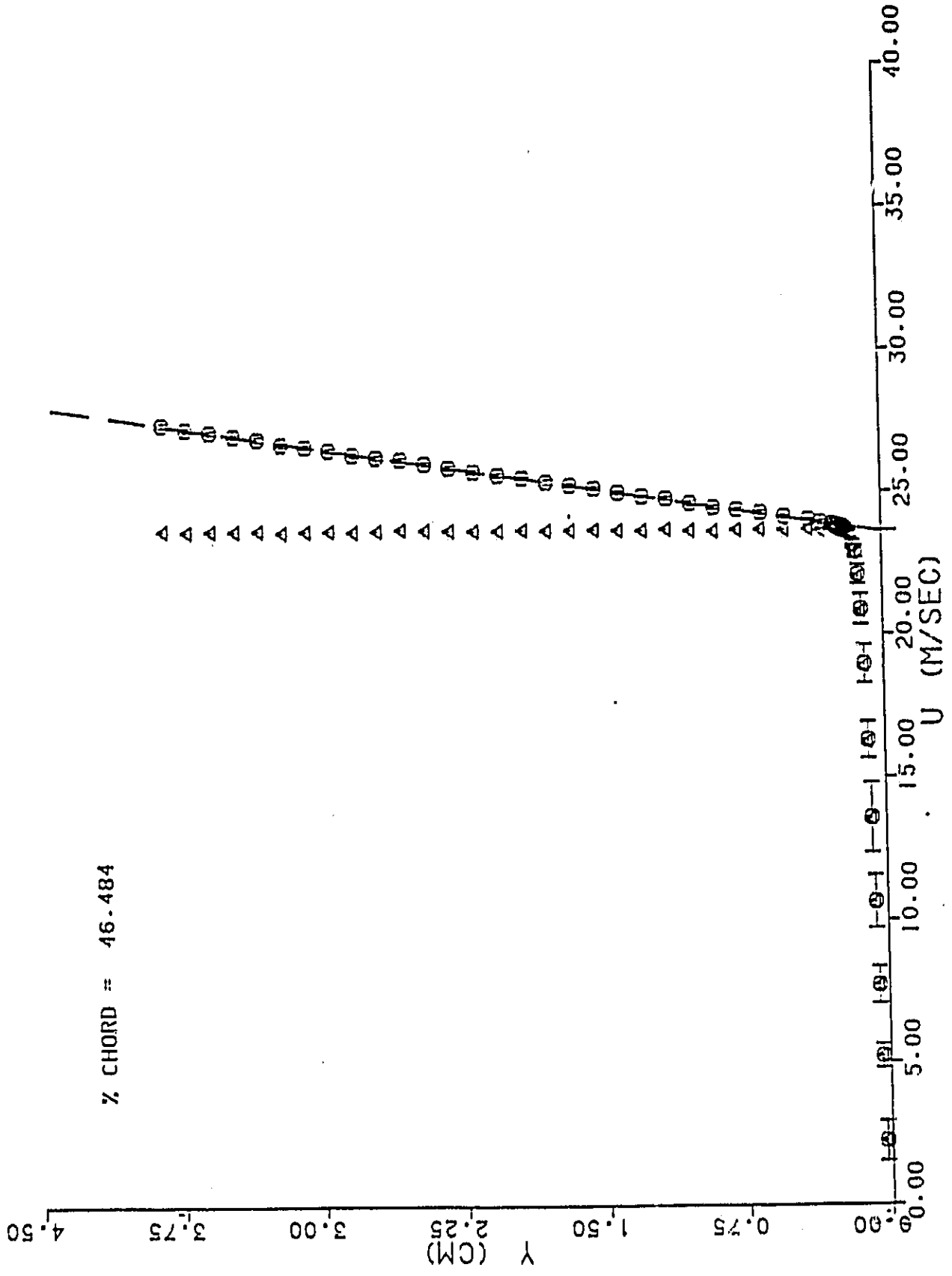
% CHORD = 46.484
Y (CM)
0.00
0.75
1.50
2.25
3.00
3.75
4.50
U (M/SEC)
0.00
5.00
10.00
15.00
20.00
25.00
30.00
35.00
40.00

Figure 16.

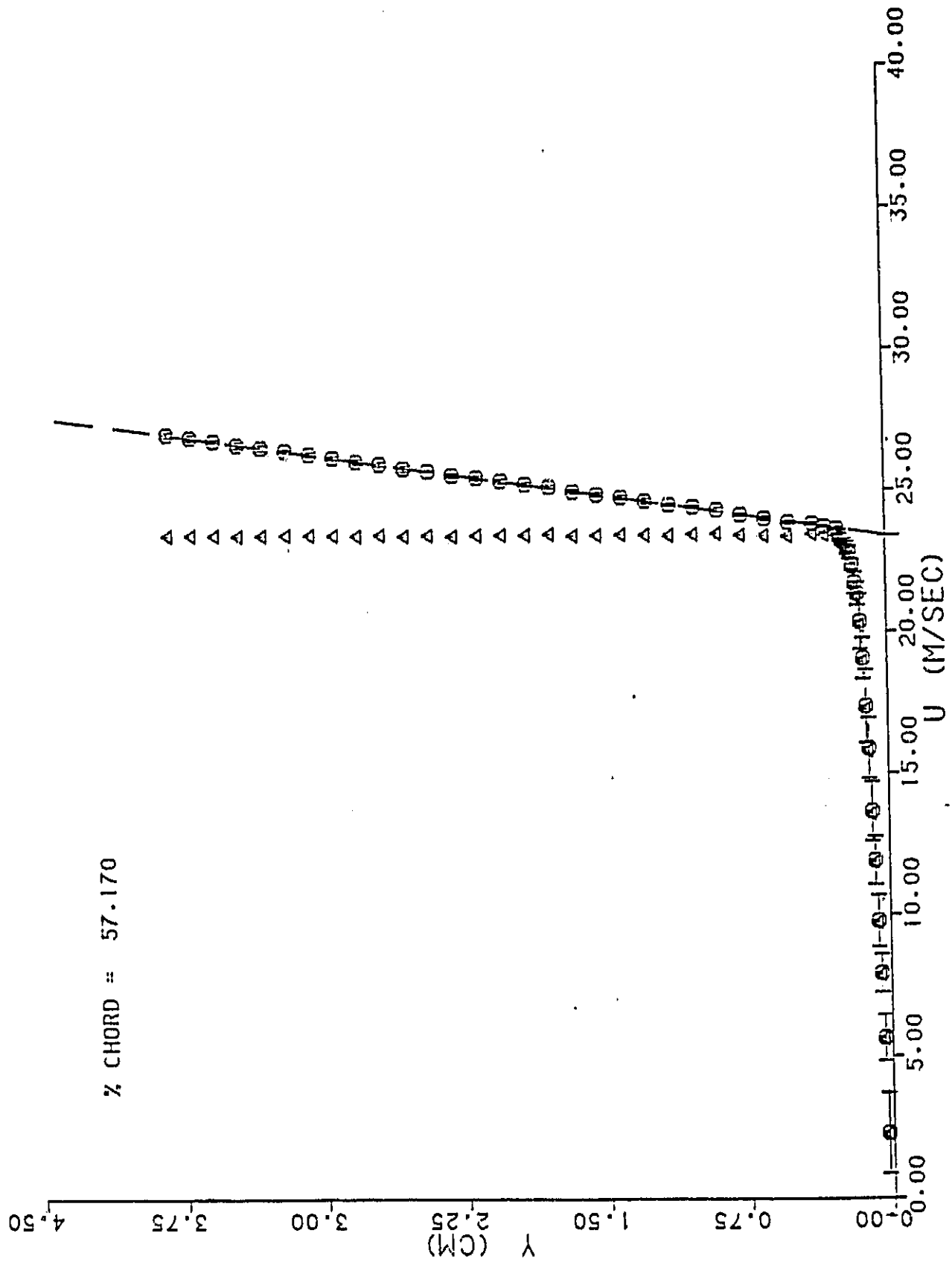
% CHORD = 57.170
Y (CM)
0.00
0.75
1.50
2.25
3.00
3.75
4.50
U (M/SEC)
0.00
5.00
10.00
15.00
20.00
25.00
30.00
35.00
40.00

Figure 17.

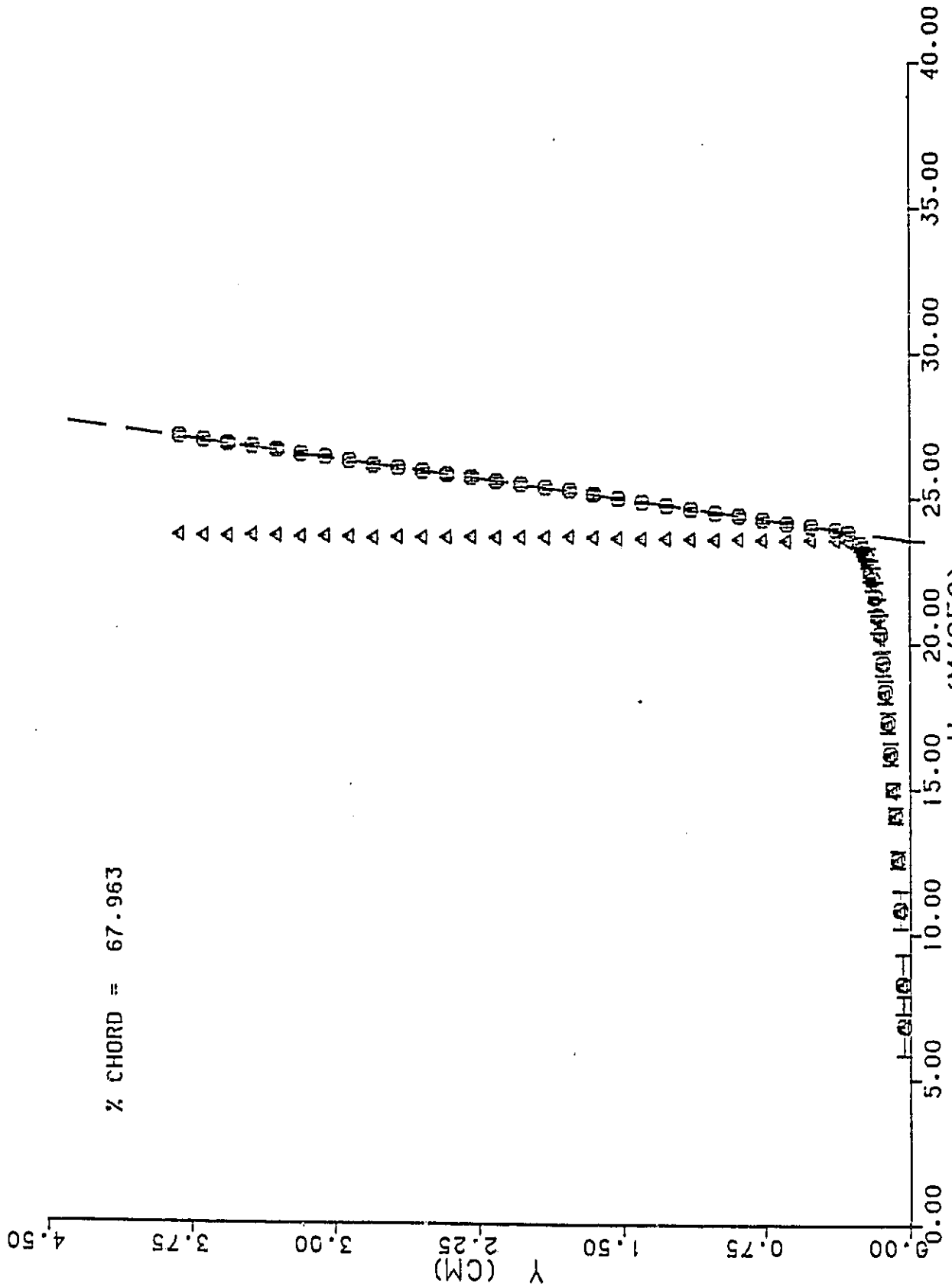
% CHORD = 67.963
Y (CM)
0.00
0.75
1.50
2.25
3.00
3.75
4.50
U (M/SEC)
0.00
5.00
10.00
15.00
20.00
25.00
30.00
35.00
40.00

Figure 18.

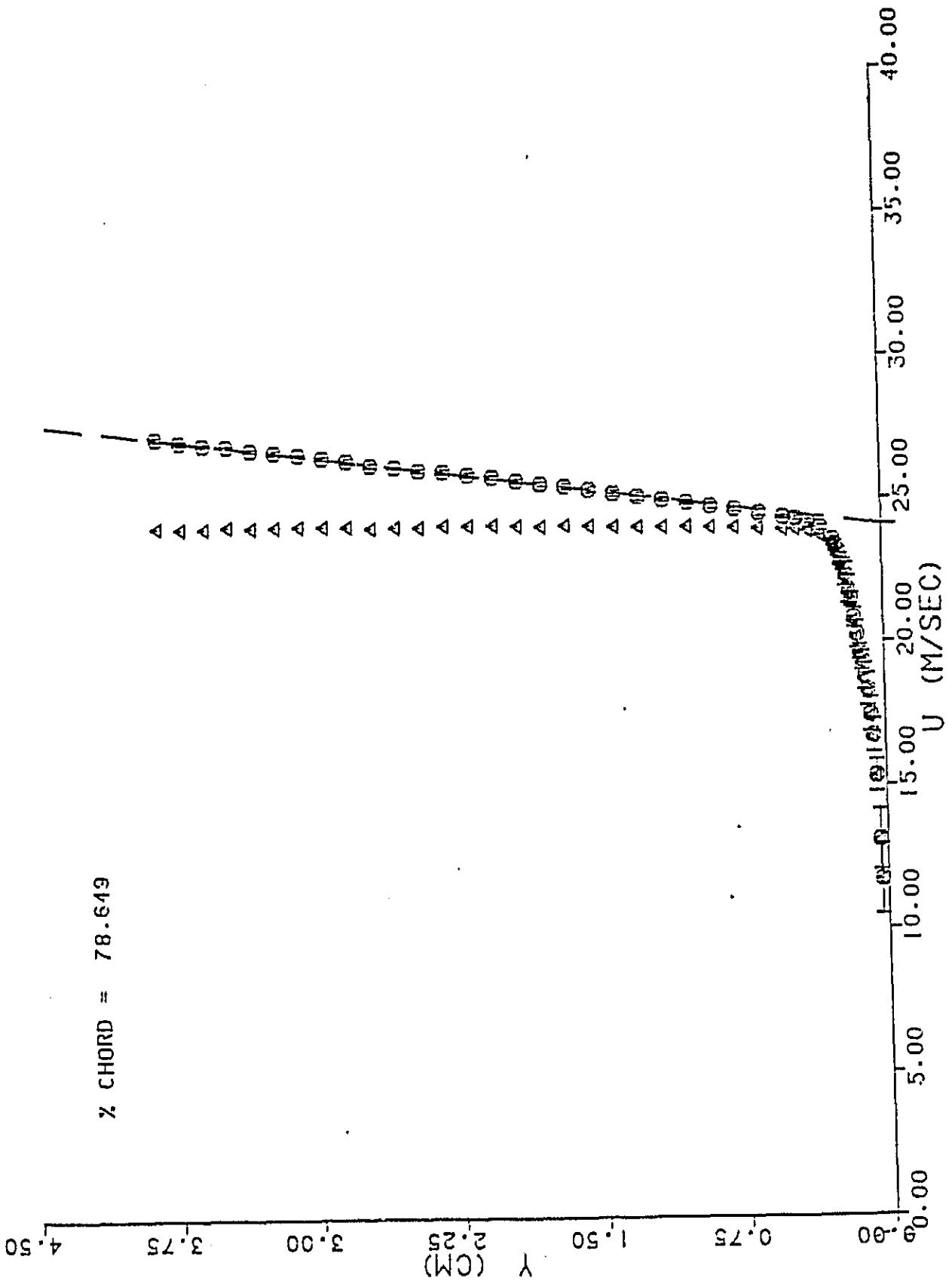
% CHORD = 78.649
Y (CM)
0.00
0.75
1.50
2.25
3.00
3.75
4.50
U (M/SEC)
0.00
5.00
10.00
15.00
20.00
25.00
30.00
35.00
40.00

Figure 19.

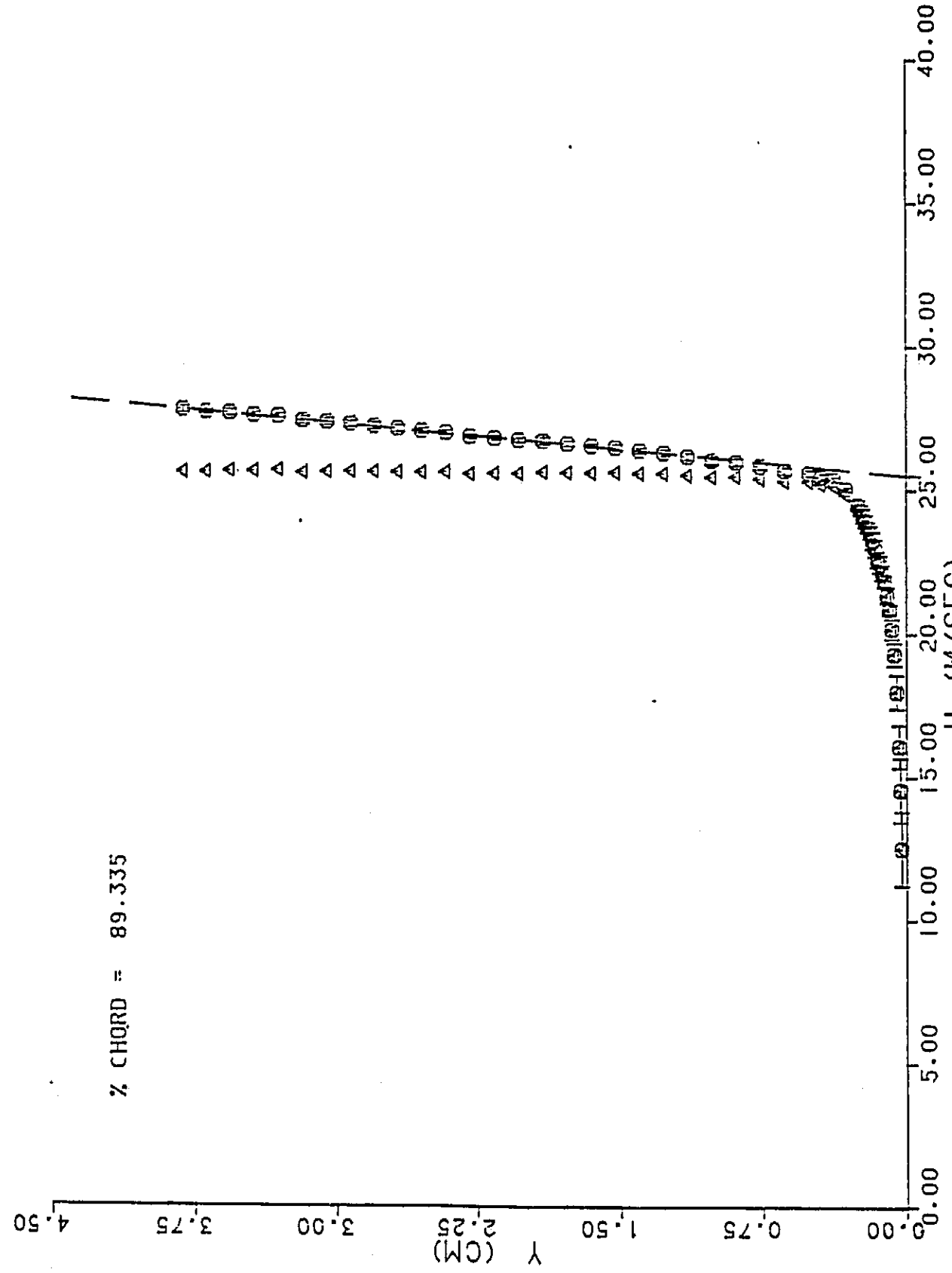
% CHORD = 89.335
Y (CM)
U (M/SEC)
0.00
0.75
1.50
2.25
3.00
3.75
4.50
0.00
5.00
10.00
15.00
20.00
25.00
30.00
35.00
40.00

Figure 20.

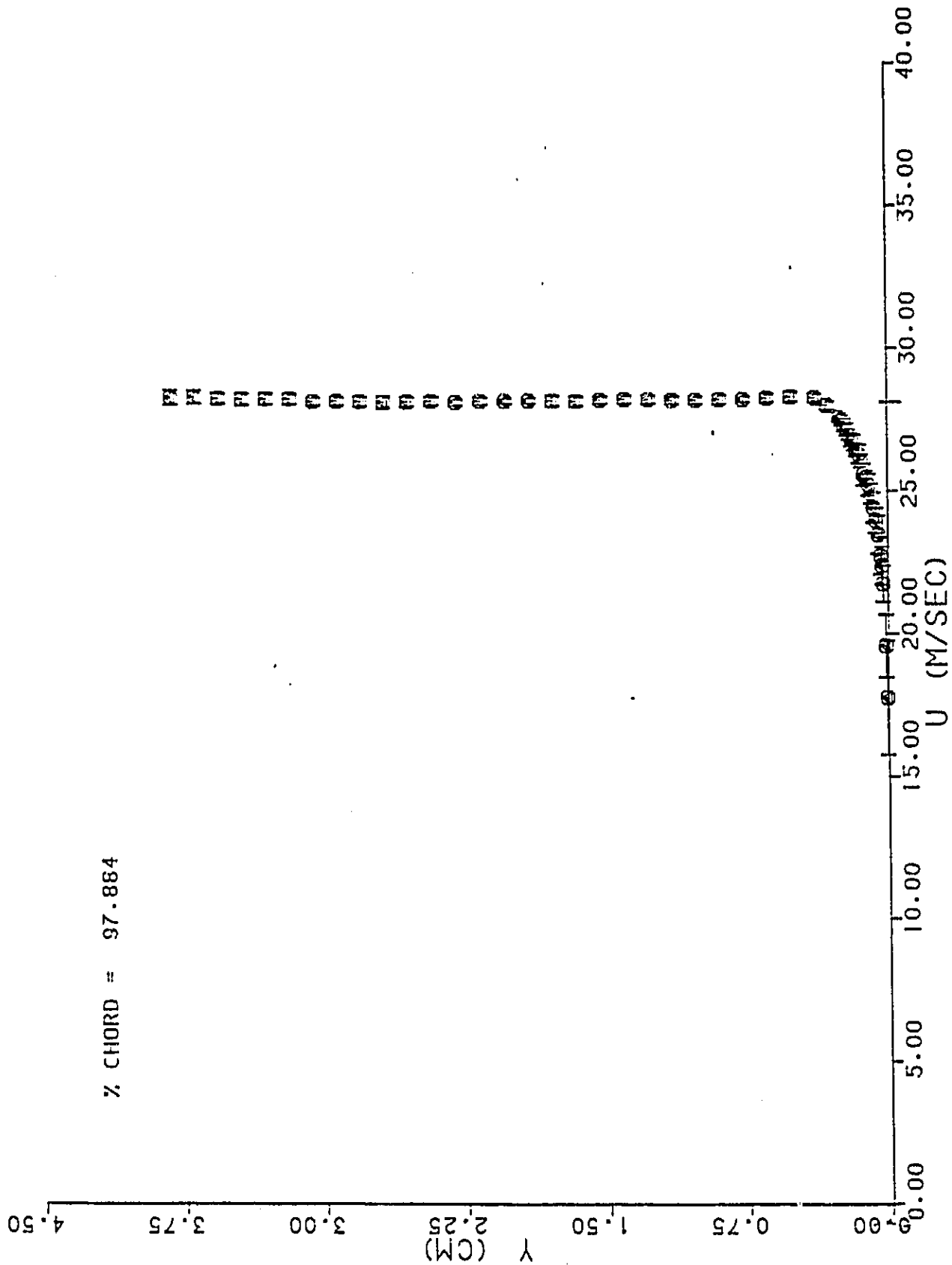
% CHORD = 97.884
Y (CM)
0.00
0.75
1.50
2.25
3.00
3.75
4.50
U (M/SEC)
0.00
5.00
10.00
15.00
20.00
25.00
30.00
35.00
40.00

Figure 21.

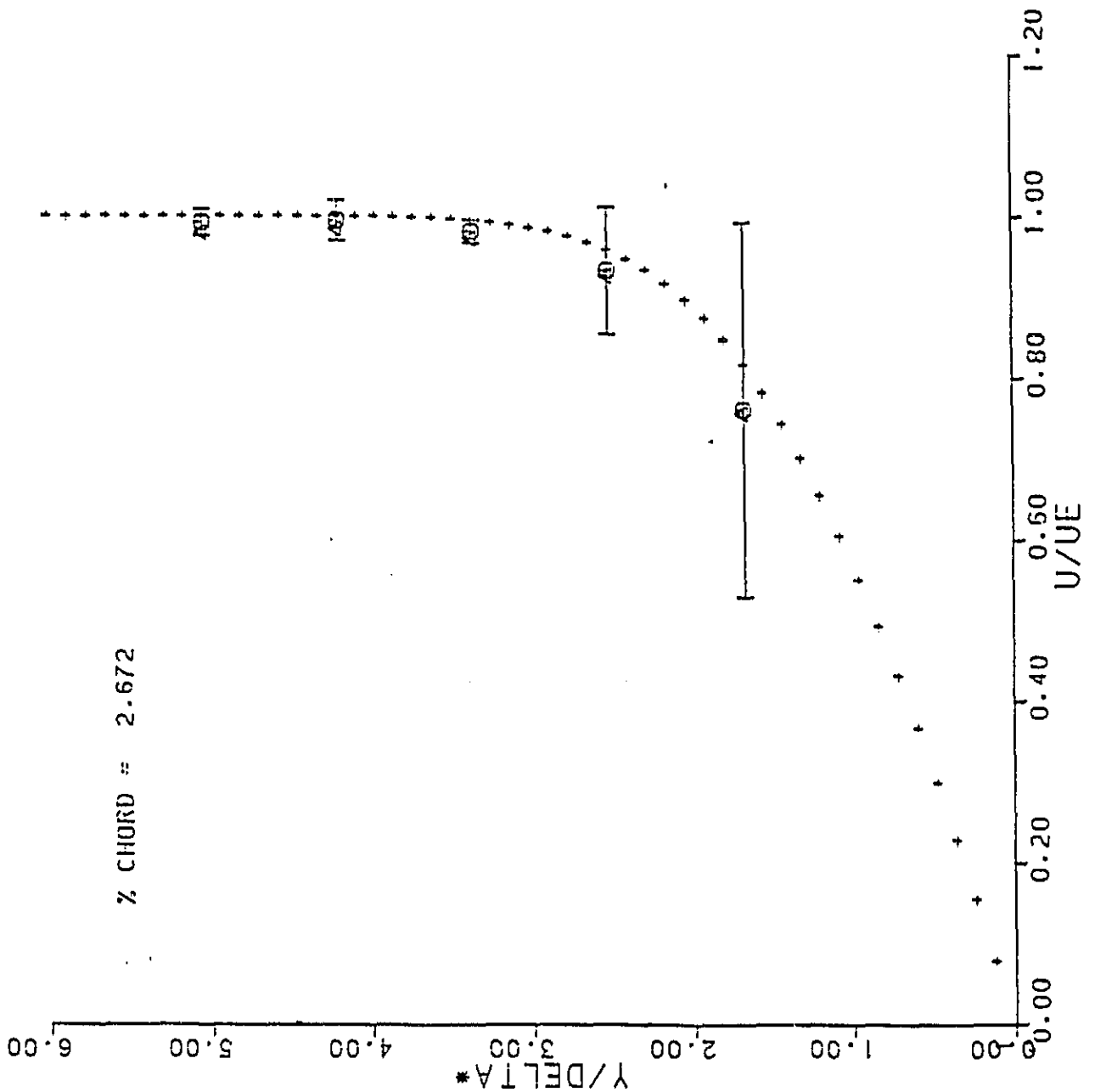
% CHORD = 2.672
Y/DELTA*
U/UE
0.00
1.00
2.00
3.00
4.00
5.00
6.00
0.00
0.20
0.40
0.60
0.80
1.00
1.20

Figure 22.

Figure 23.

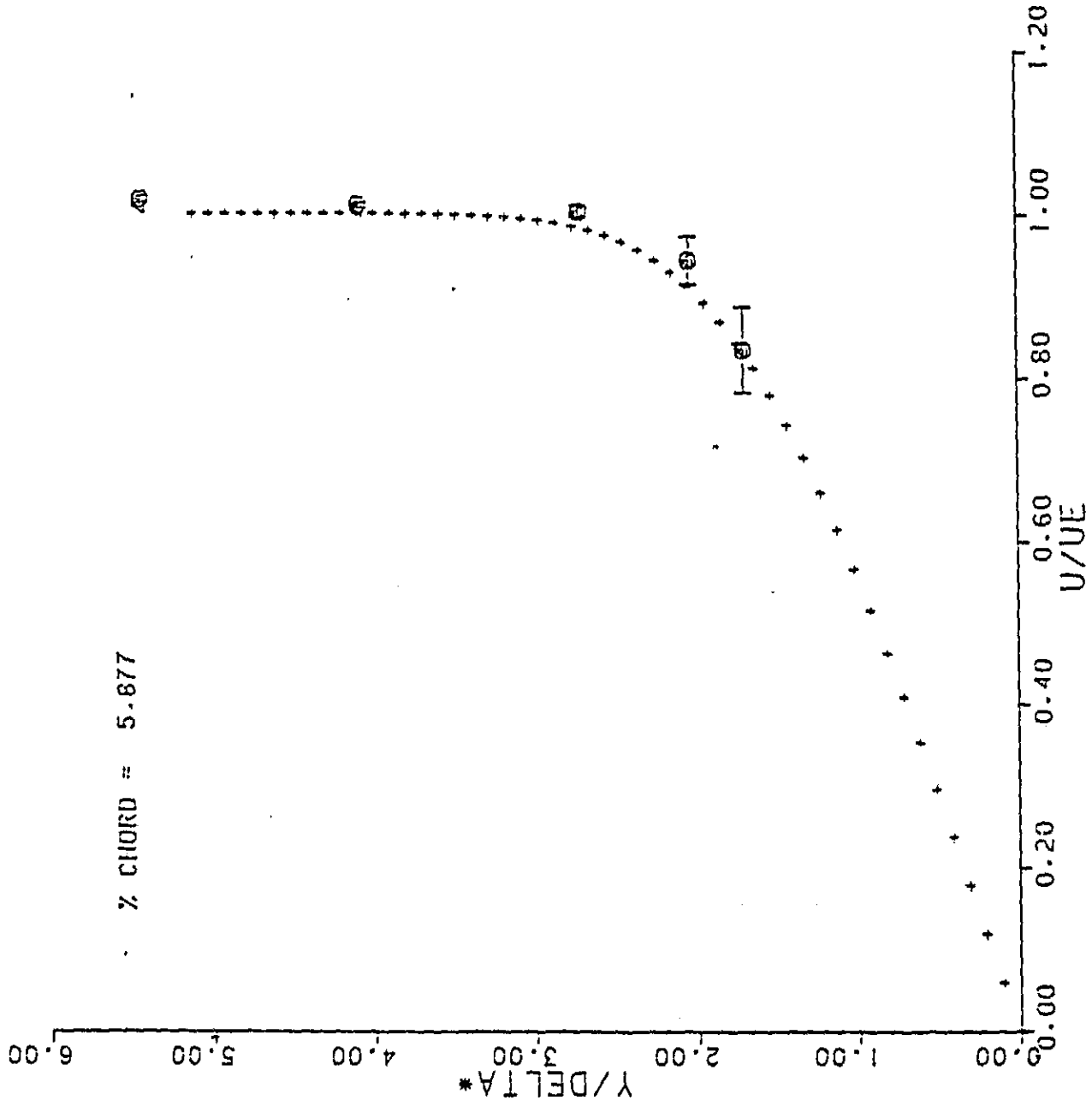
% CHORD = 5.877
Y/DELTA*
U/UE
0.00
1.00
2.00
3.00
4.00
5.00
6.00
0.00
0.20
0.40
0.60
0.80
1.00
1.20

Figure 24.

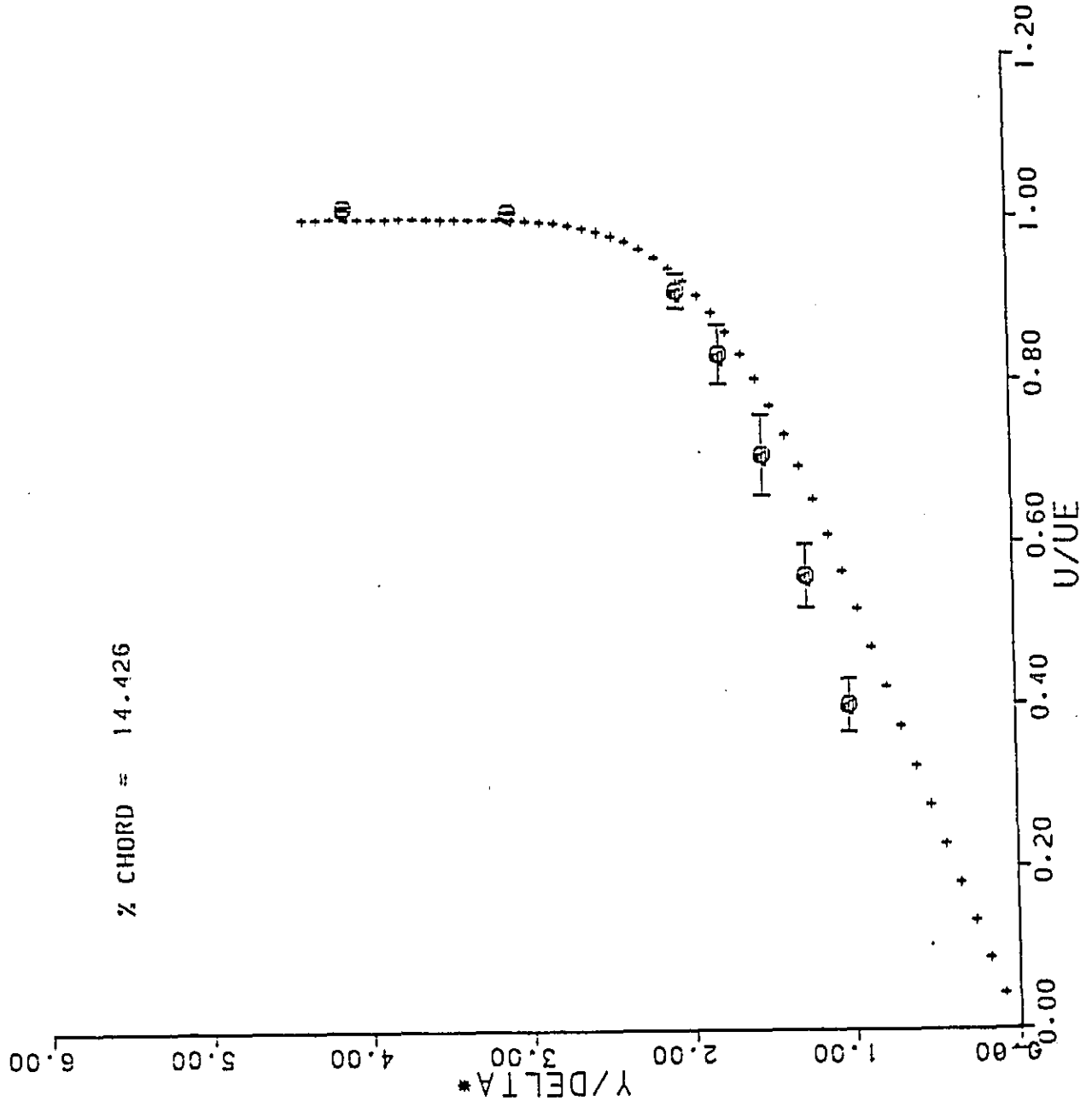
% CHORD = 14.426
Y/DELTA*
0.00
1.00
2.00
3.00
4.00
5.00
6.00
0.00
0.20
0.40
0.60
0.80
1.00
1.20
U/UE

Figure 25.

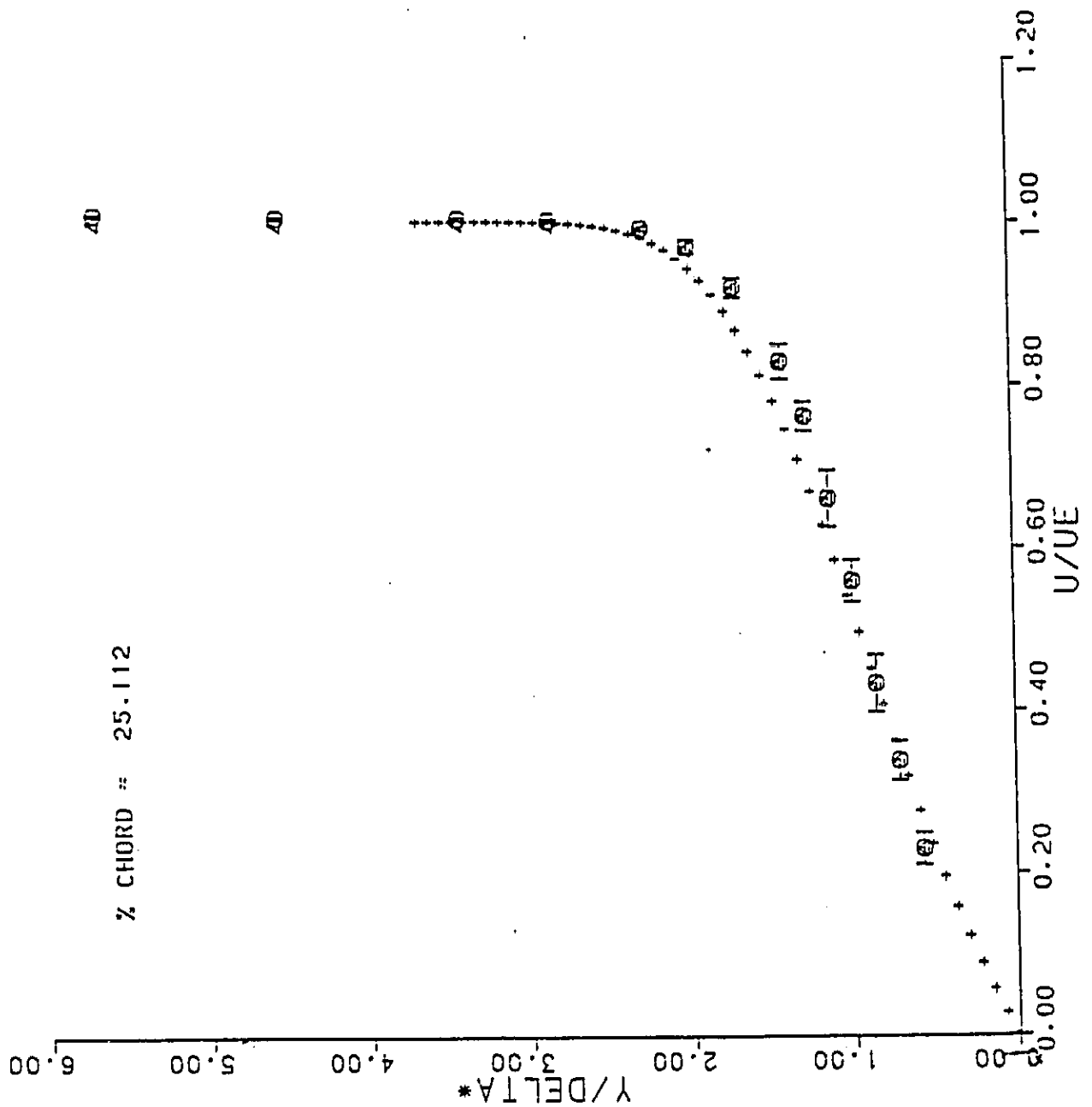
% CHORD = 25.112
Y/DELTA*
U/UE
0.00
1.00
2.00
3.00
4.00
5.00
6.00
0.00
0.20
0.40
0.60
0.80
1.00
1.20

Figure 26.

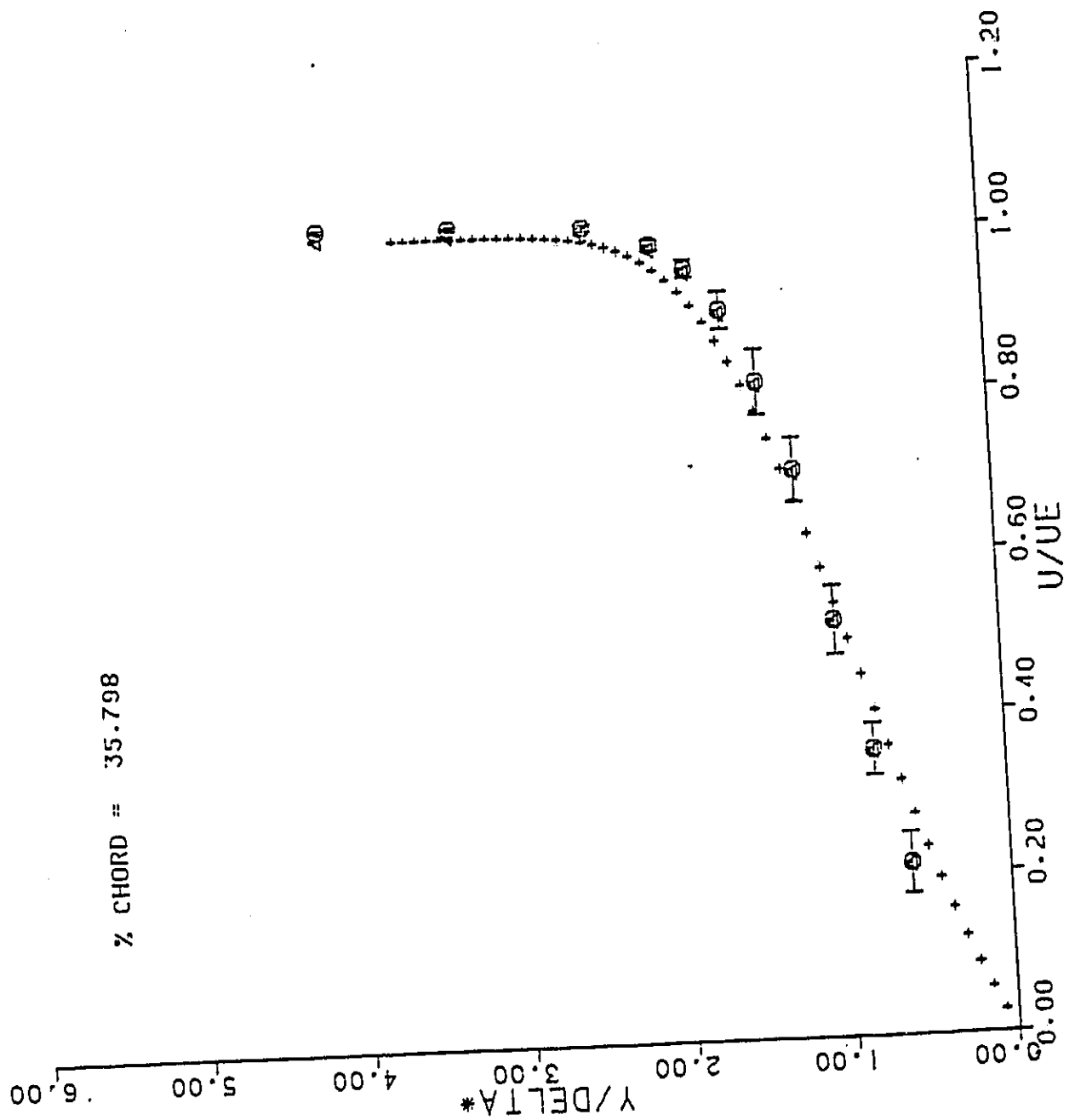
% CHORD = 35.798
Y/DELTA*
U/UE
0.00
1.00
2.00
3.00
4.00
5.00
6.00
0.00
0.20
0.40
0.60
0.80
1.00
1.20

Figure 27.

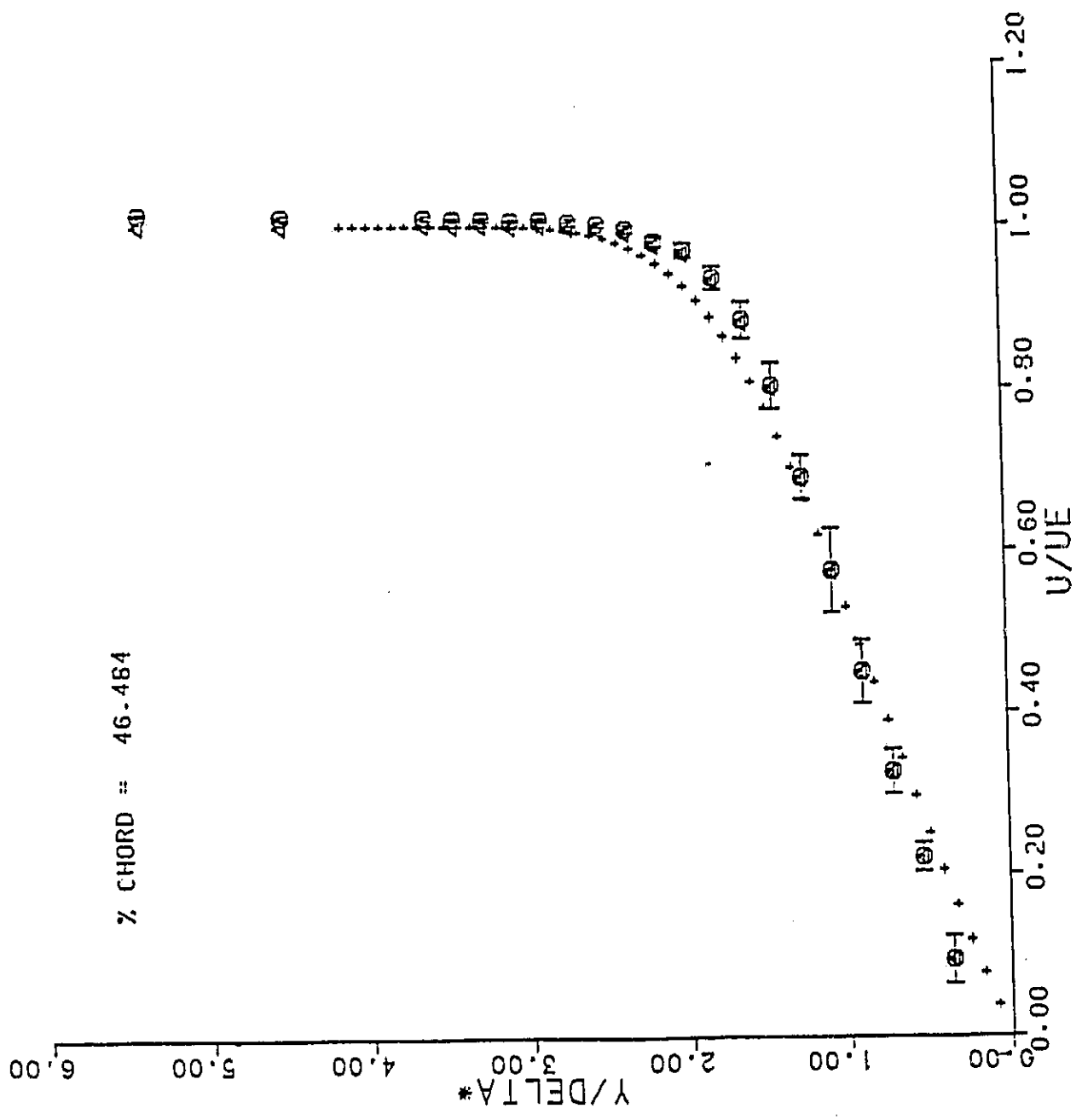
% CHORD = 46.464
Y/DELTA*
U/UE
0.00
0.20
0.40
0.60
0.80
1.00
1.20
1.00
2.00
3.00
4.00
5.00
6.00

Figure 28.

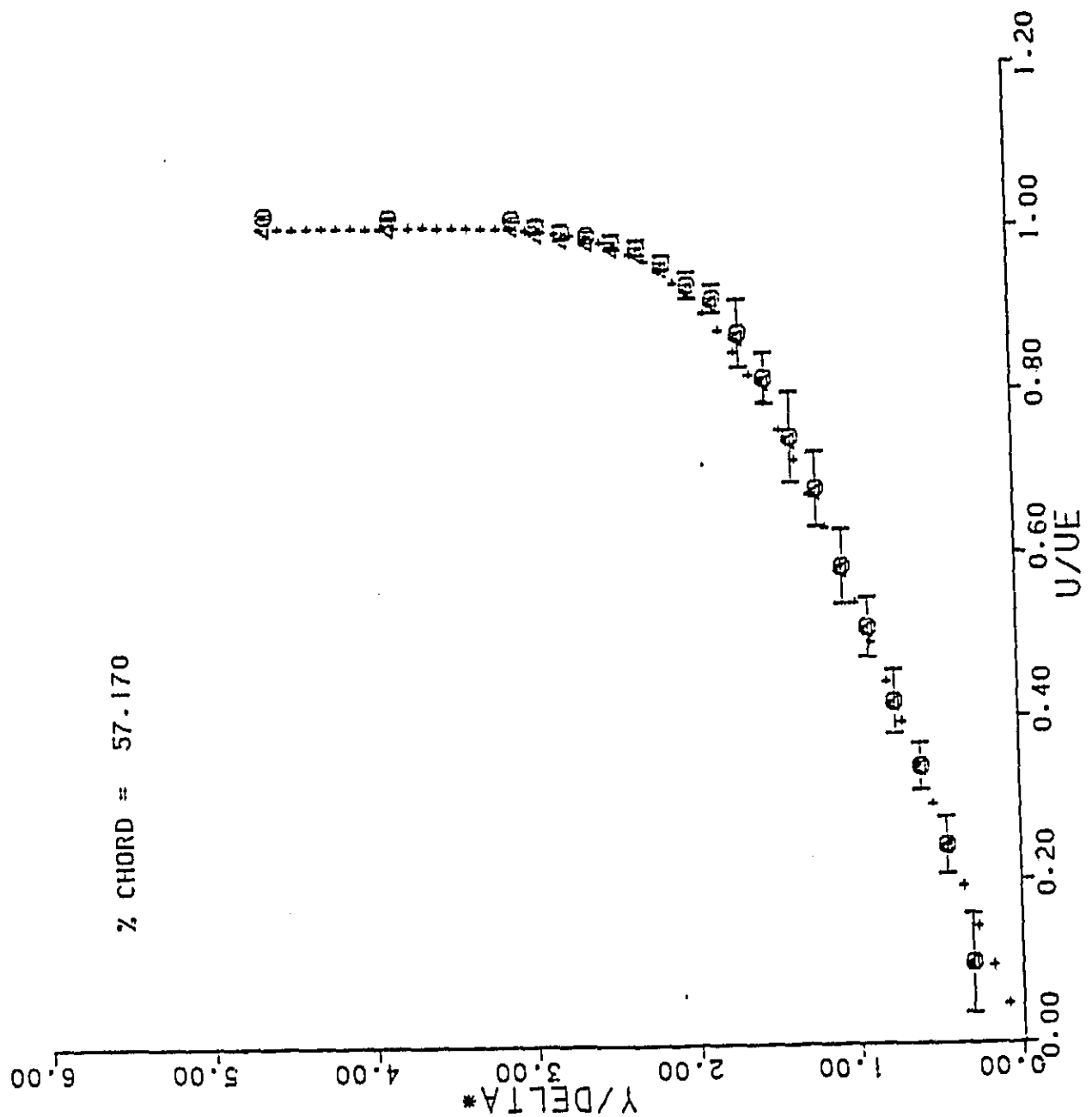
% CHORD = 57.170
Y/DELTA*
U/UE
0.00
1.00
2.00
3.00
4.00
5.00
6.00
0.00
0.20
0.40
0.60
0.80
1.00
1.20

Figure 29.

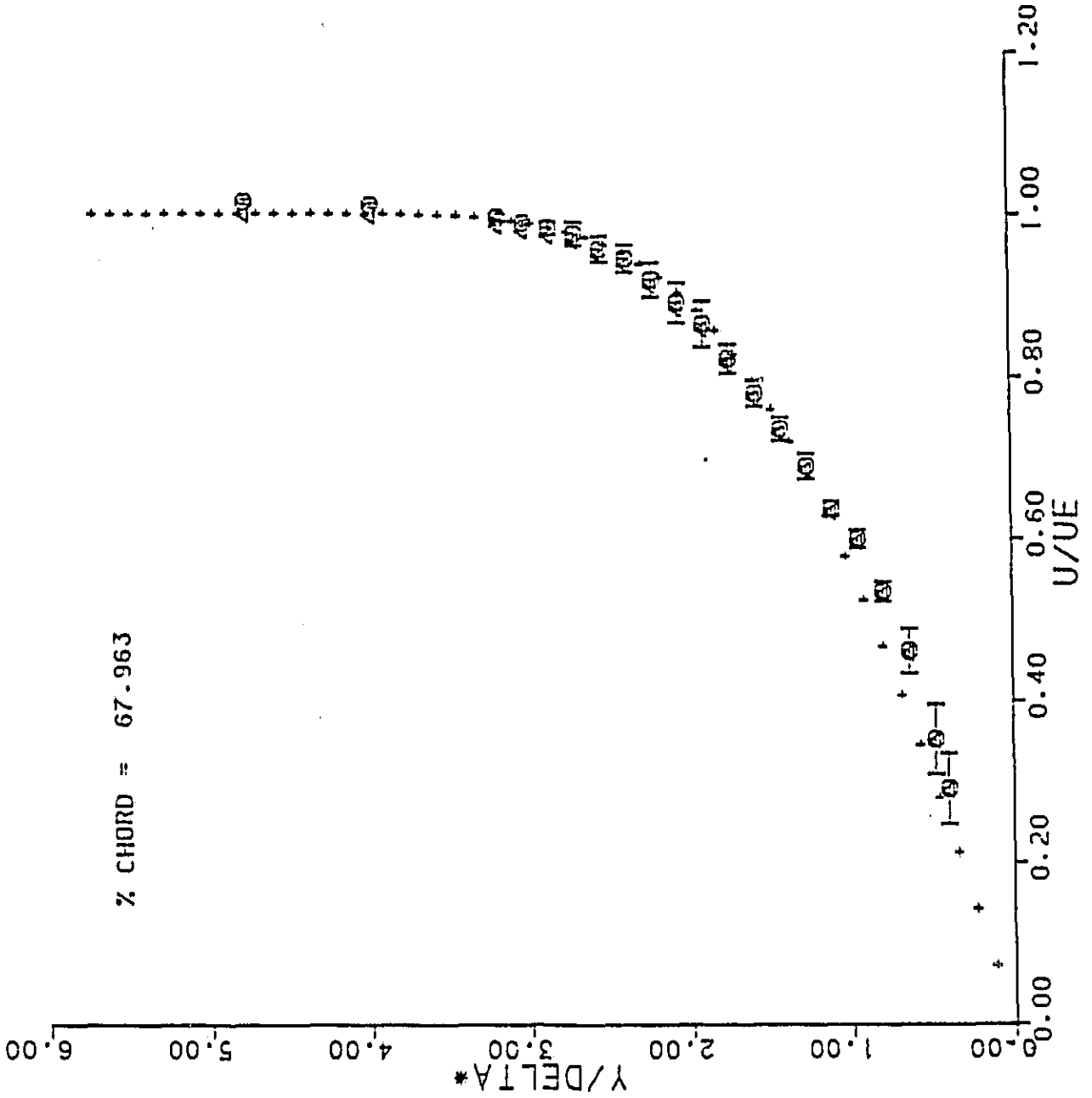
% CHORD = 67.963
Y/DELTA*
U/UE
0.00
1.00
2.00
3.00
4.00
5.00
6.00
0.00
0.20
0.40
0.60
0.80
1.00
1.20

Figure 30.

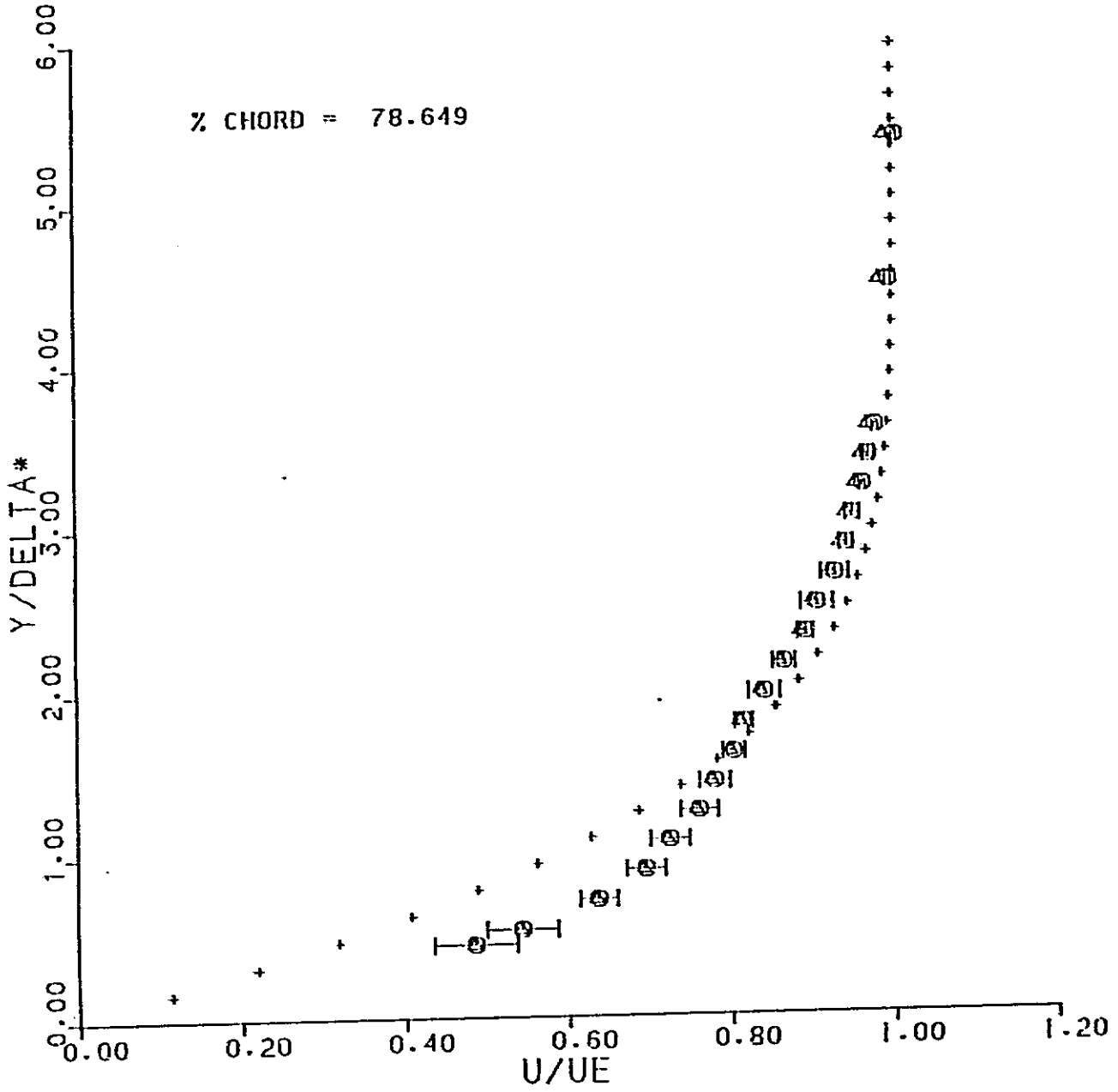
% CHORD = 78.649
Y/DELTA*
U/UE
0.00
1.00
2.00
3.00
4.00
5.00
6.00
0.00
0.20
0.40
0.60
0.80
1.00
1.20

Figure 31.

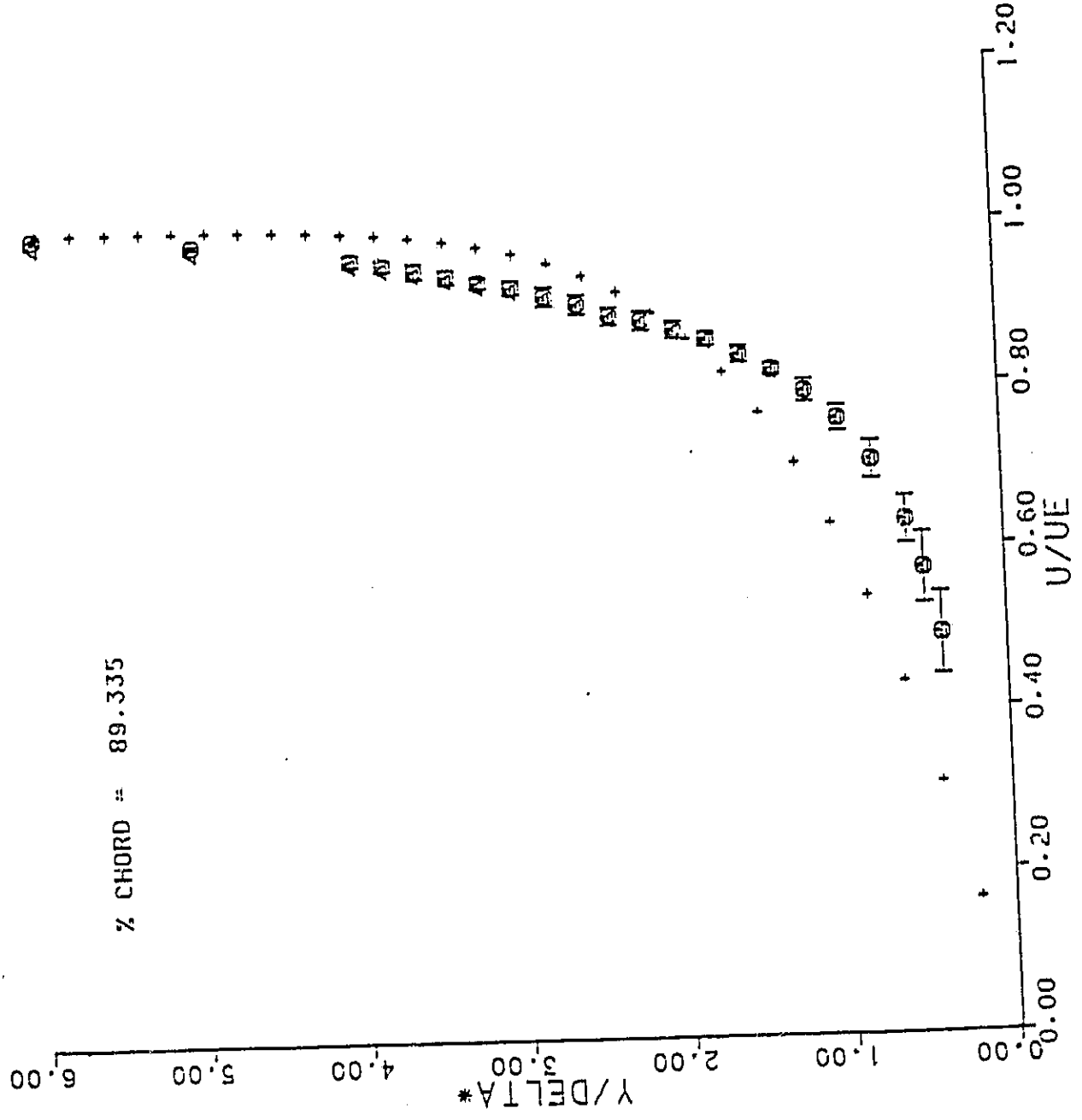
% CHORD = 89.335
Y/DELTA*
U/UE
0.00
1.00
2.00
3.00
4.00
5.00
6.00
0.00
0.20
0.40
0.60
0.80
1.00
1.20

Figure 32.

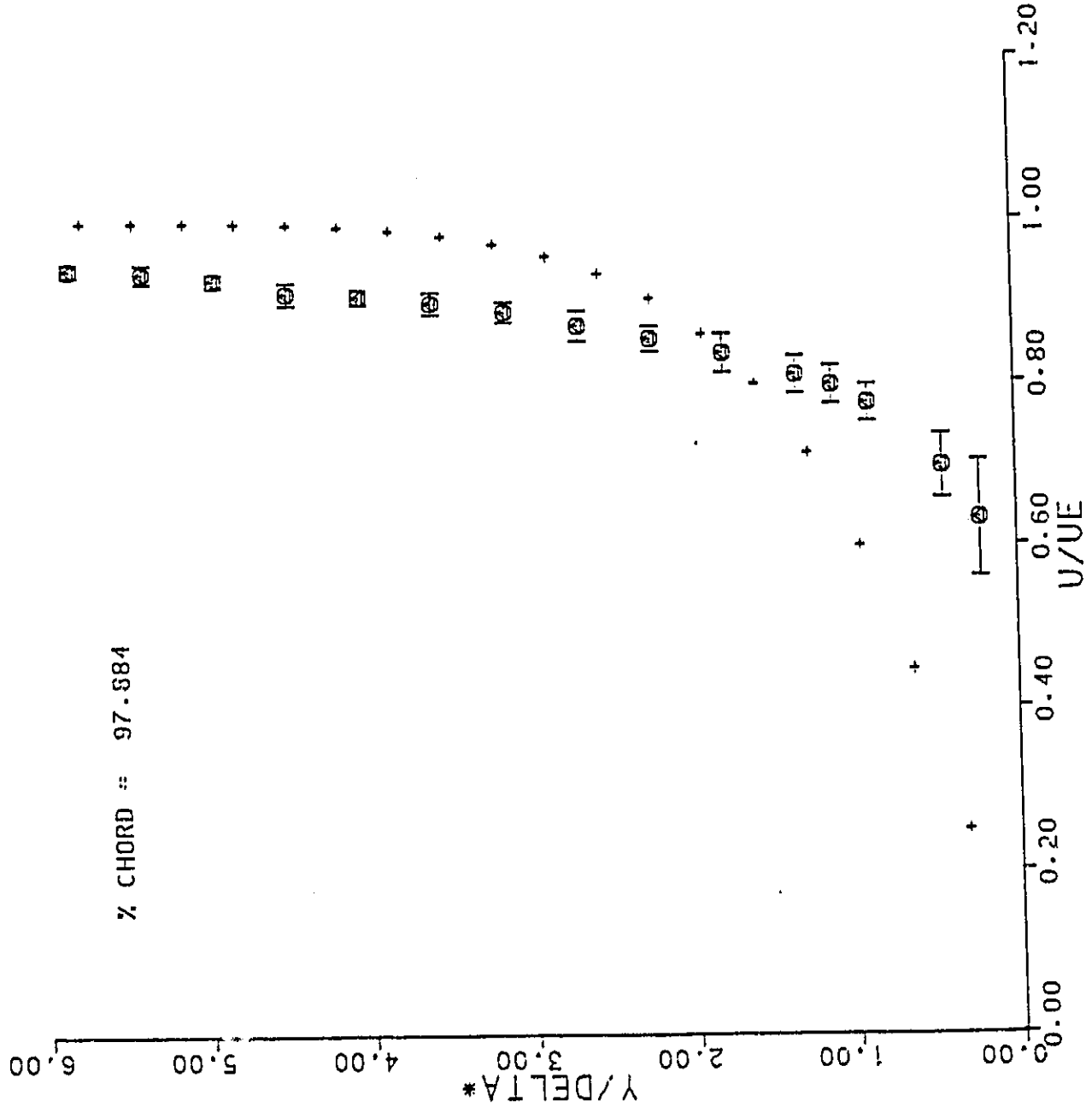
% CHORD = 97.584
Y/DELTA*
U/UE
0.00
1.00
2.00
3.00
4.00
5.00
6.00
0.00
0.20
0.40
0.60
0.80
1.00
1.20

Figure 33.

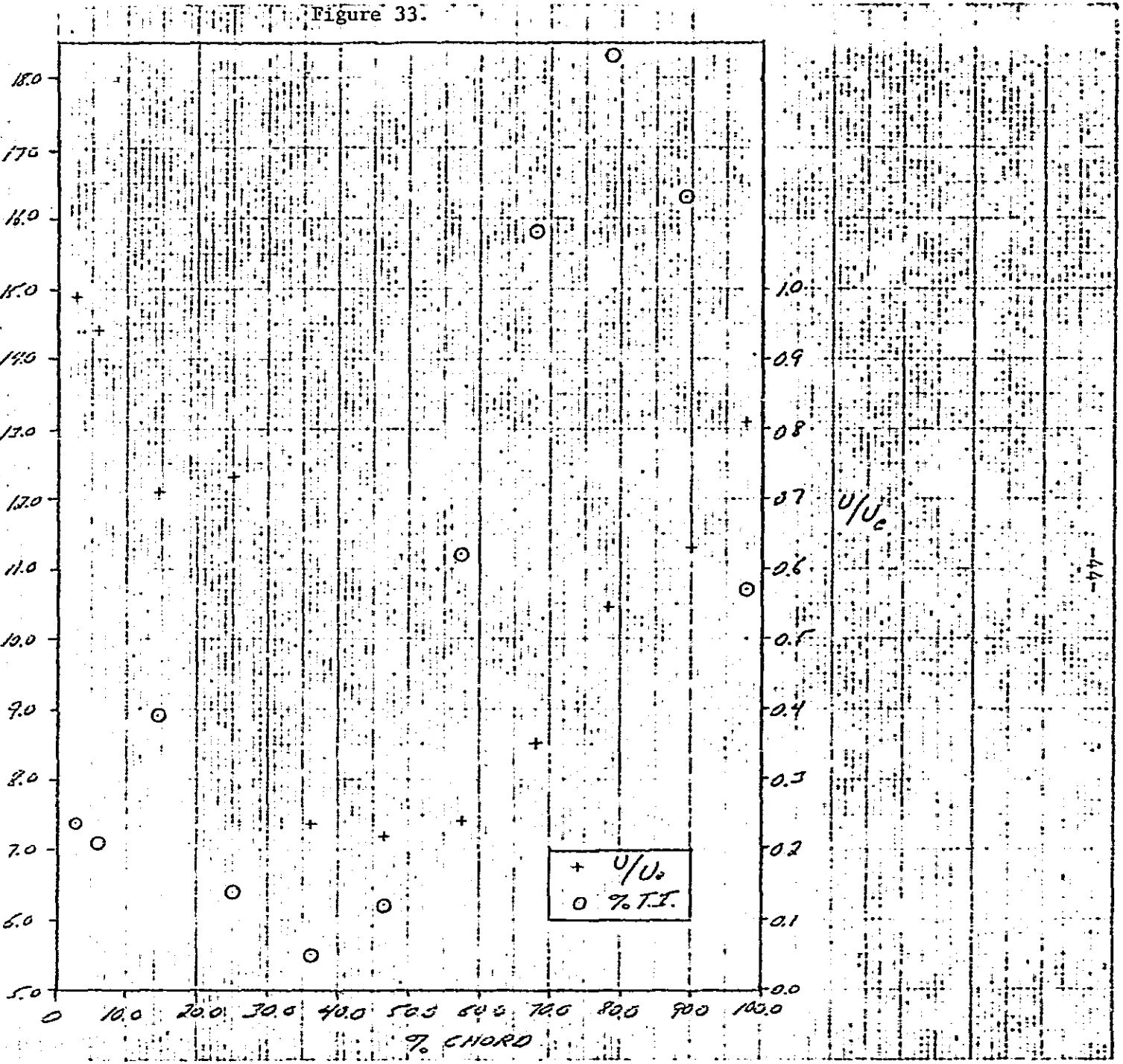

Figure 34.

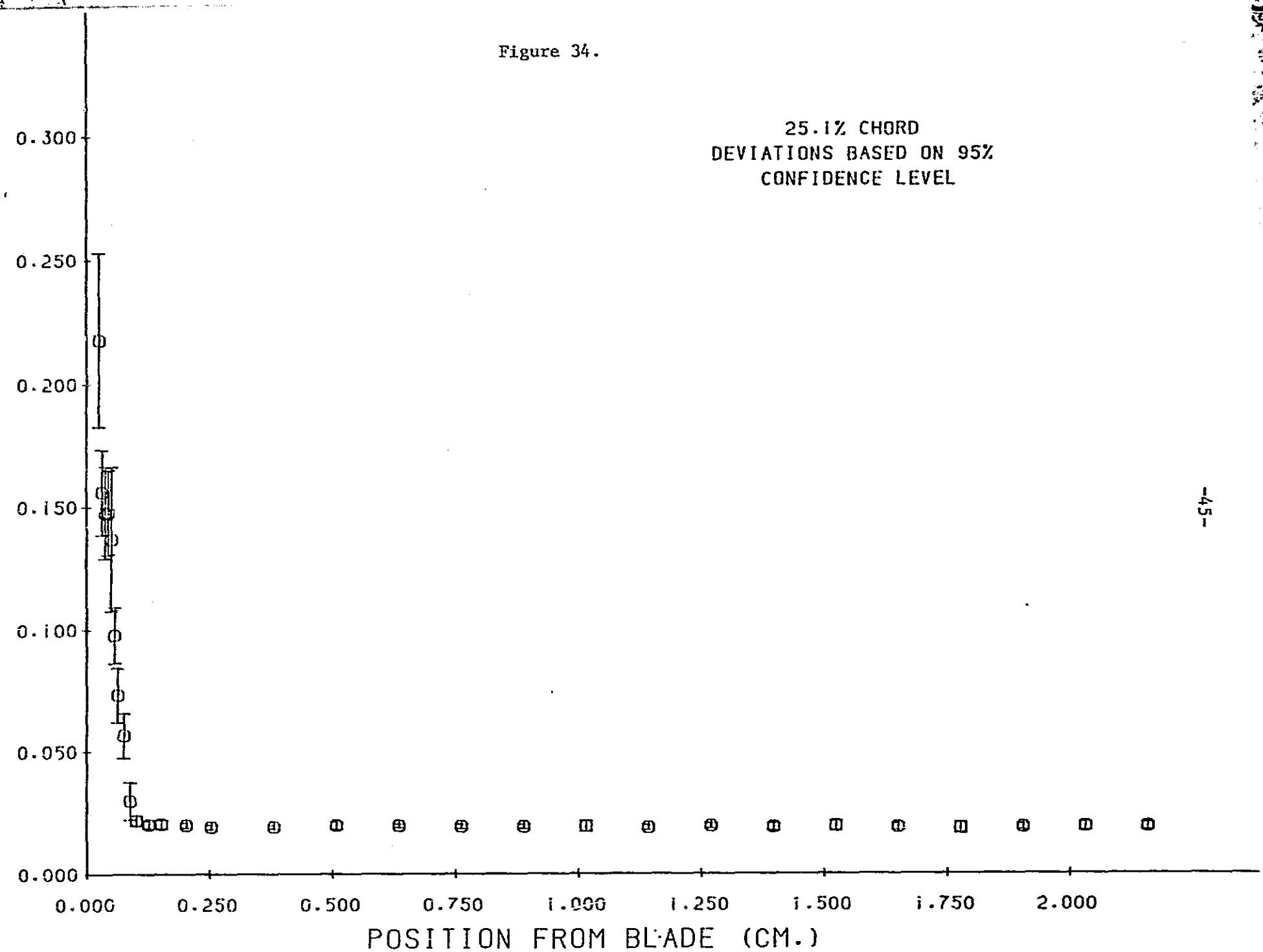
25.1% CHORD
DEVIATIONS BASED ON 95%
CONFIDENCE LEVEL
0.300
0.250
0.200
0.150
0.100
0.050
0.000
0.000
0.250
0.500
0.750
1.000
1.250
1.500
1.750
2.000
POSITION FROM BLADE (CM.)

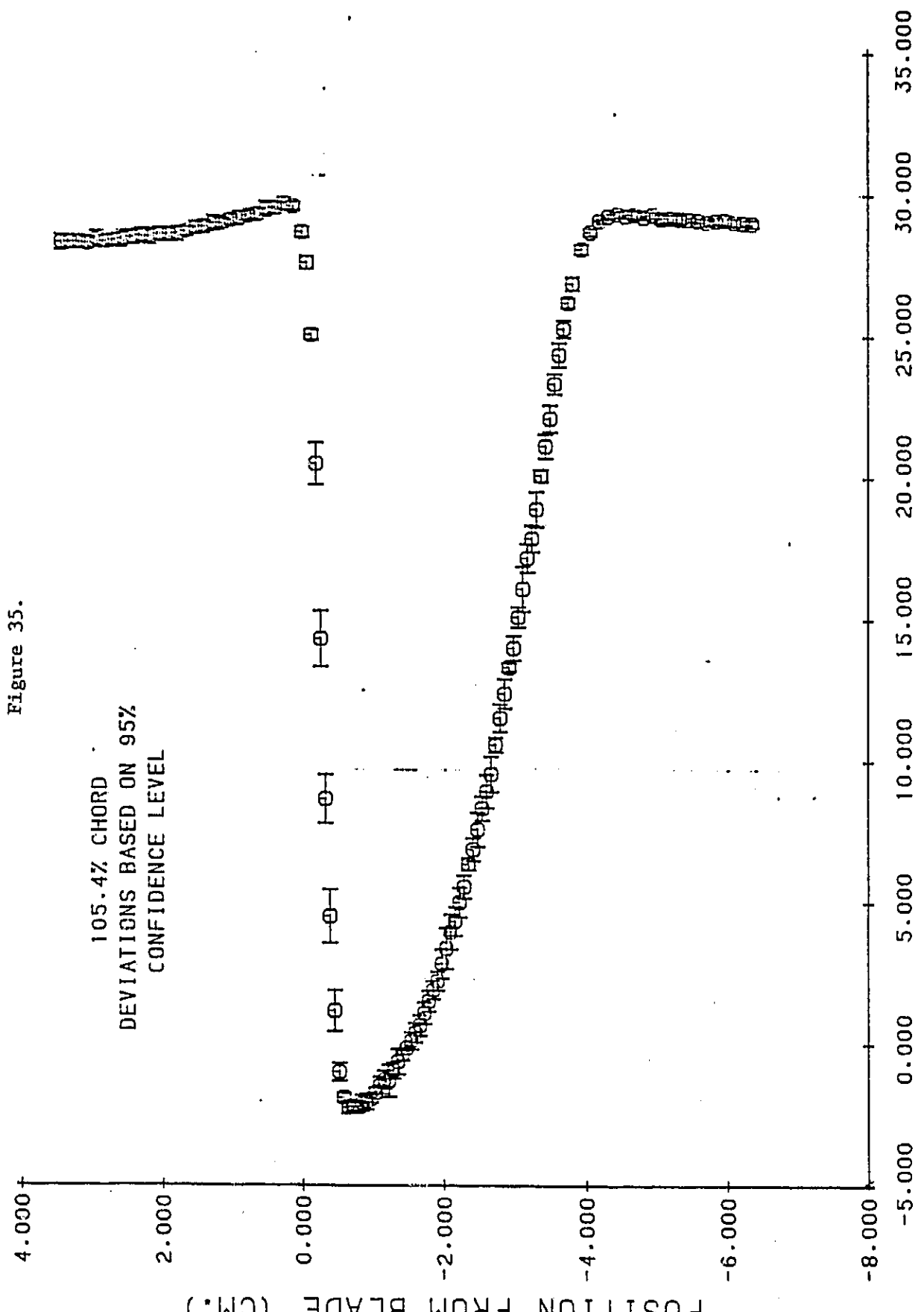
105.4% CHORD
DEVIATIONS BASED ON 95%
CONFIDENCE LEVEL
POSITION FROM BLADE (CM.)
4.000
2.000
0.000
-2.000
-4.000
-6.000
-8.000
-5.000
0.000
5.000
10.000
15.000
20.000
25.000
30.000
35.000
U (M/SEC)

Figure 35.

Figure 36.

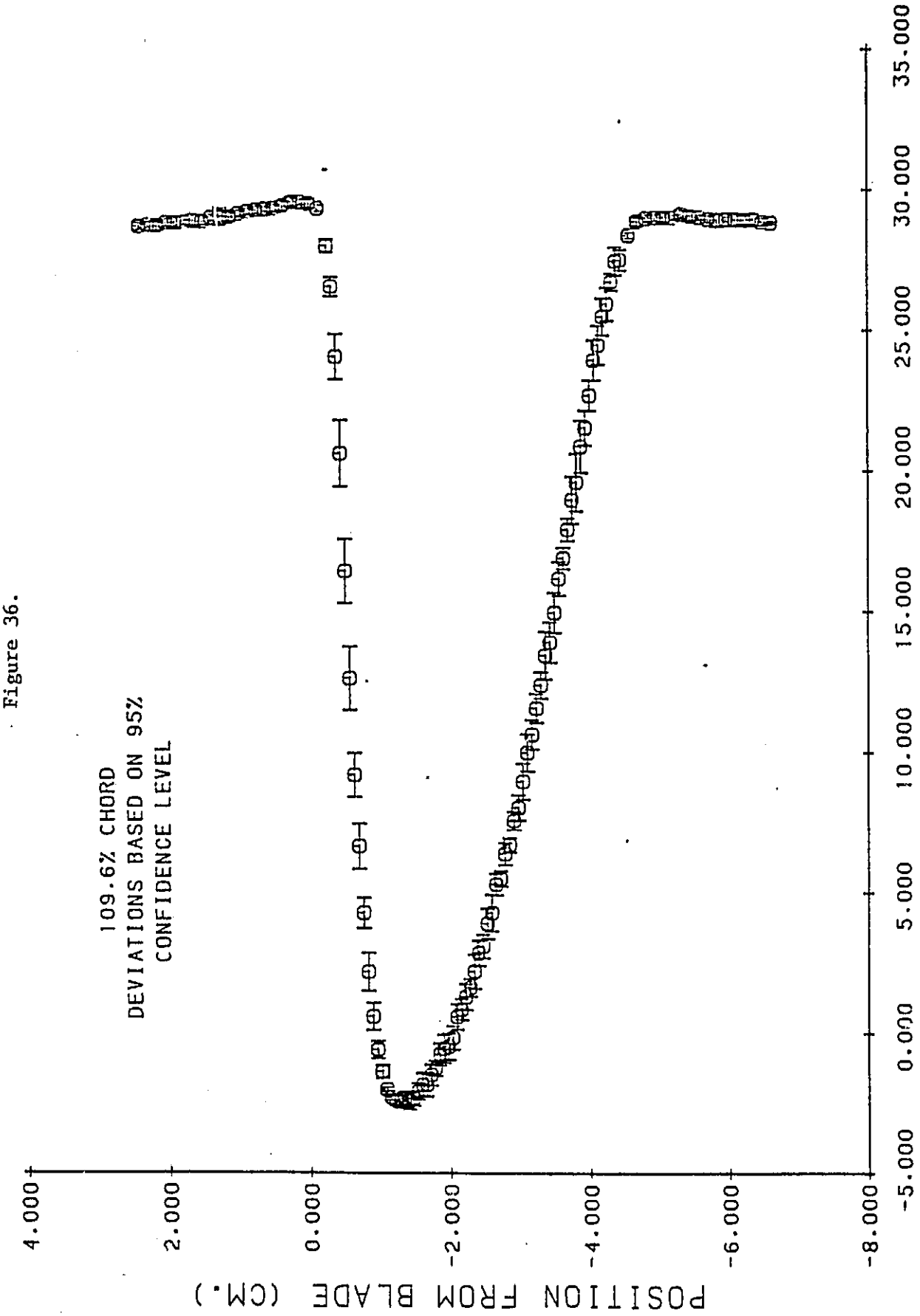
109.6% CHORD
DEVIATIONS BASED ON 95%
CONFIDENCE LEVEL
POSITION FROM BLADE (CM.)
4.000
2.000
0.000
-2.000
-4.000
-6.000
-8.000
-5.000
0.000
5.000
10.000
15.000
20.000
25.000
30.000
35.000
U (M/SEC)

Figure 34.

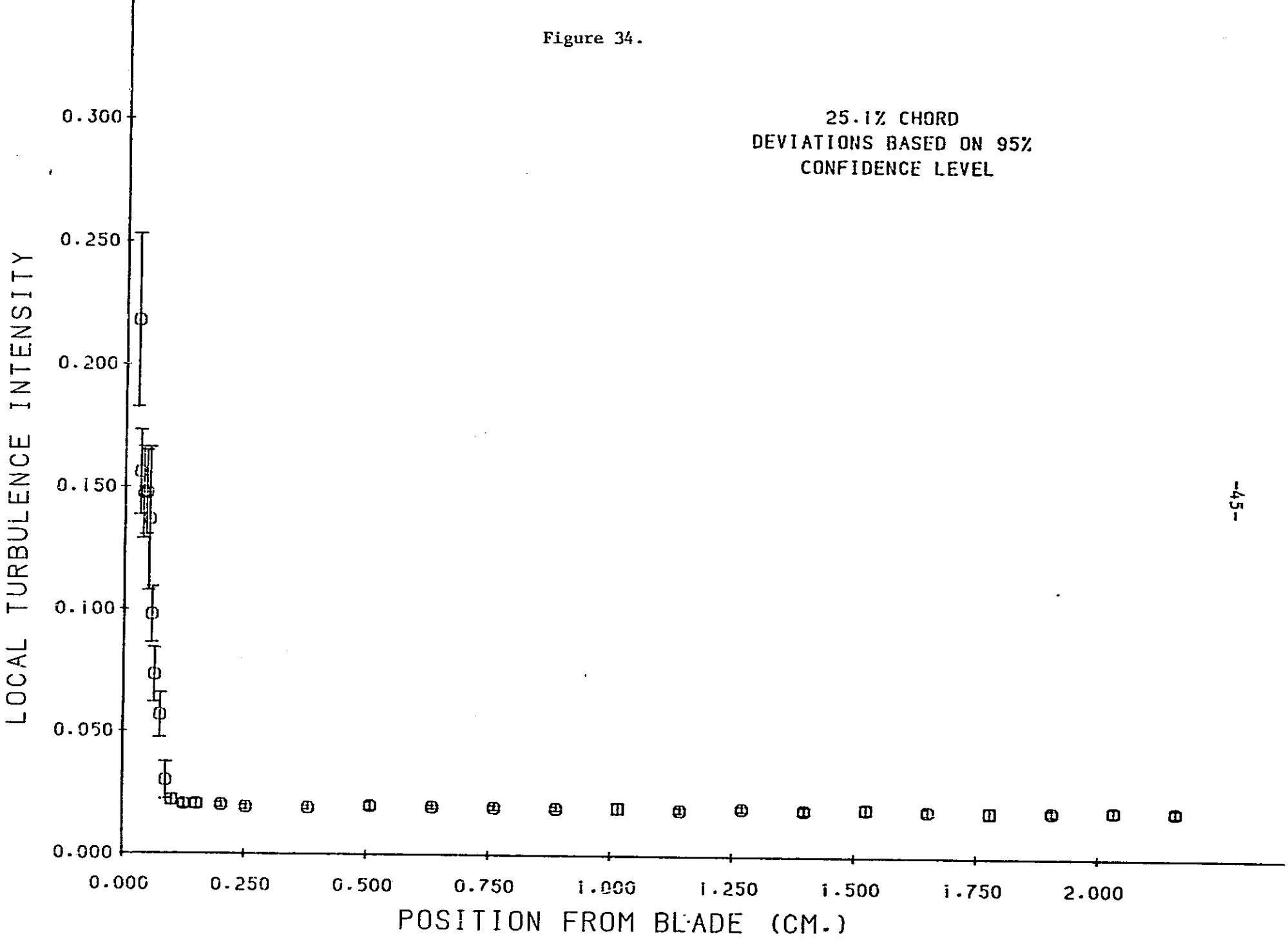
25.1% CHORD
DEVIATIONS BASED ON 95%
CONFIDENCE LEVEL
LOCAL TURBULENCE INTENSITY
0.300
0.250
0.200
0.150
0.100
0.050
0.000
0.000
0.250
0.500
0.750
1.000
1.250
1.500
1.750
2.000
POSITION FROM BLADE (CM.)